2
Nuclear Reactions

2.1
Cross Sections

The cross section σ is a quantitative measure for the probability that an interaction will occur. In the following we define several quantities which are displayed in Fig. 2.1. Suppose that a beam of $\mathcal{N}_b$ particles per unit time t, covering an area A, is incident on a target. The number of *nonoverlapping* target nuclei within the beam is $\mathcal{N}_t$. We assume that the total number of interactions that occur per unit time, $\mathcal{N}_R/t$, is equal to the total number of emitted (nonidentical) interaction products per unit time, $\mathcal{N}_e/t$. If the interaction products are scattered incident particles, then we are referring to elastic scattering. If the interaction products have an identity different from the incident particles, then we are referring to a reaction. The number of interaction products emitted at an angle θ with respect to the beam direction into the solid angle $d\Omega$ is $\mathcal{N}_e^{d\Omega}$. The area perpendicular to the direction θ covered by a radiation detector is given by $dF = r^2\, d\Omega$. The cross section is defined by

$$\sigma \equiv \frac{\left(\text{number of interactions per time}\right)}{\left(\text{number of incident particles per area per time}\right)\left(\text{number of target nuclei within the beam}\right)}$$
$$= \frac{(\mathcal{N}_R/t)}{[\mathcal{N}_b/(tA)]\,\mathcal{N}_t} \tag{2.1}$$

We will use this general definition to describe reaction probabilities in astrophysical plasmas and in laboratory measurements of nuclear reactions. In the latter case, two situations are frequently encountered: (i) if the beam area, A, is larger than the target area, A_t, then

$$\frac{\mathcal{N}_R}{t} = \frac{\mathcal{N}_b}{tA}\,\mathcal{N}_t\sigma \tag{2.2}$$

and the number of reactions per unit time is expressed in terms of the incident *particle flux*, $\mathcal{N}_b/(tA)$, the number of target nuclei, $\mathcal{N}_t$, and the cross section; (ii) if the target area, A_t, is larger than the beam area, A, then

$$\frac{\mathcal{N}_R}{t} = \frac{\mathcal{N}_b}{t}\frac{\mathcal{N}_t}{A}\,\sigma \tag{2.3}$$

Nuclear Physics of Stars. Christian Iliadis

ISBN: 978-3-527-40602-9

and the number of reactions per unit time is expressed in terms of the incident *particle current*, $\mathcal{N}_b/t$, the total number of target nuclei within the beam per area covered by the beam, $\mathcal{N}_t/A$, and the cross section. Of course, for a homogeneous target, $\mathcal{N}_t/A$ is equal to the *total* number of target nuclei divided by the *total* target area A_t. The latter quantity is easier to determine in practice. We can also express the total cross section, σ, and the differential cross section, $d\sigma/d\Omega$, in terms of the number of emitted interaction products

$$\frac{\mathcal{N}_e}{t} = \sigma \frac{(\mathcal{N}_b/t)}{A}\,\mathcal{N}_t \tag{2.4}$$

$$\frac{\mathcal{N}_e^{d\Omega}}{t} = \left(\frac{d\sigma}{d\Omega}\right)\frac{(\mathcal{N}_b/t)}{A}\,\mathcal{N}_t\,d\Omega \tag{2.5}$$

If we define $\mathcal{N}_{et} \equiv \mathcal{N}_e/\mathcal{N}_t$, that is, the number of emitted interaction products per target nucleus, then we obtain

$$\sigma = \frac{(\mathcal{N}_{et}/t)}{(\mathcal{N}_b/t)(1/A)} \qquad \text{and} \qquad \left(\frac{d\sigma}{d\Omega}\right) = \frac{(\mathcal{N}_{et}^{d\Omega}/t)}{(\mathcal{N}_b/t)(1/A)}\frac{1}{d\Omega} \tag{2.6}$$

With the definition of a flux or current density j as the number of particles per time per area, we can write for the beam and emitted interaction products

$$j_b = \frac{(\mathcal{N}_b/t)}{A} \tag{2.7}$$

$$j_{et} = \frac{(\mathcal{N}_{et}^{d\Omega}/t)}{dF} \tag{2.8}$$

For the total and differential cross section one finds

$$\sigma = \frac{(\mathcal{N}_{et}/t)}{j_b} \tag{2.9}$$

$$\left(\frac{d\sigma}{d\Omega}\right) = \frac{j_{et}\,dF}{j_b\,d\Omega} = \frac{j_{et}r^2\,d\Omega}{j_b\,d\Omega} = \frac{j_{et}r^2}{j_b} \tag{2.10}$$

These quantities are related by

$$\sigma = \int \left(\frac{d\sigma}{d\Omega}\right) d\Omega \tag{2.11}$$

Common units of nuclear reaction and scattering cross sections are

$$1\,\mathrm{b} \equiv 10^{-24}\,\mathrm{cm}^2 = 10^{-28}\,\mathrm{m}^2$$
$$1\,\mathrm{fm}^2 = (10^{-15}\,\mathrm{m})^2 = 10^{-30}\,\mathrm{m}^2 = 10^{-2}\,\mathrm{b}$$

In this chapter, all kinematic quantities are given in the center-of-mass system (Appendix C), unless noted otherwise.

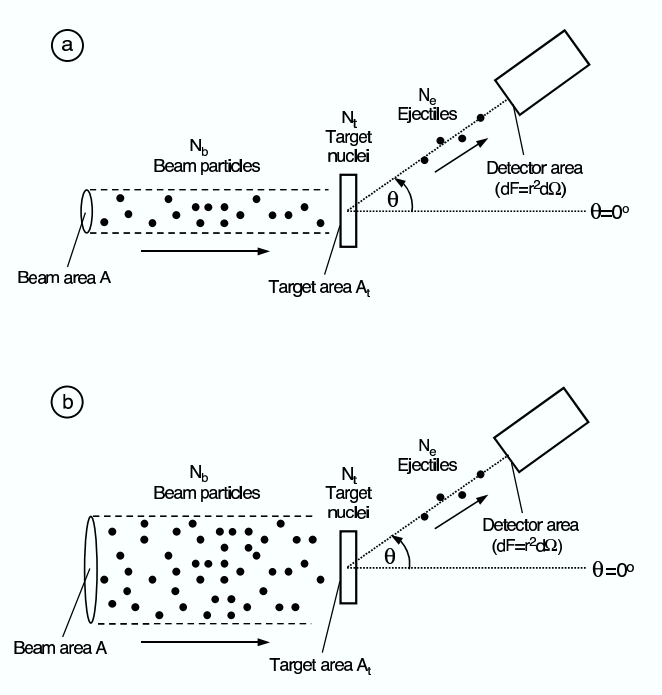

Fig. 2.1 Typical nuclear physics counting experiment, showing a beam of $\mathcal{N}_b$ particles per unit time, $\mathcal{N}_t$ nonoverlapping target nuclei within the beam area A, $\mathcal{N}_e$ interaction products and a detector of area dF. The detector is located at an angle of θ with respect to the incident beam direction. The two situations correspond to as follows: (a) the target area is larger than the beam area; and (b) the beam area is larger than the target area.

2.2 Reciprocity Theorem

Consider the reaction $A + a \rightarrow B + b$, where A and a denote the target and projectile, respectively, and B and b are the reaction products. The cross section of this reaction is fundamentally related to that of the reverse reaction, $B + b \rightarrow A + a$, since these processes are invariant under time-reversal, that is, the direction of time does not enter explicitly in the equations describing these processes. At a given total energy, the corresponding cross sections $\sigma_{Aa\rightarrow Bb}$ and $\sigma_{Bb\rightarrow Aa}$ are not equal but are simply related by the phase space available in the exit channel or, equivalently, by the number of final states per unit energy interval in each case. The number of states available for momenta between p and $p + dp$ is proportional to p^2 (Messiah 1999). Hence

$$\sigma_{Aa\rightarrow Bb} \sim p_{Bb}^2 \qquad \text{and} \qquad \sigma_{Bb\rightarrow Aa} \sim p_{Aa}^2 \tag{2.12}$$

The linear momentum and the de Broglie wavelength are related by $\lambda = h/p$. The wave number k of the free particle is defined in terms of the de Broglie wavelength by $\lambda \equiv 2\pi/k$. Hence, we have $p = mv = \hbar k$. It follows (Blatt and Weisskopf 1952) that

$$\frac{k_{Aa}^2 \sigma_{Aa\to Bb}}{(1+\delta_{Aa})} = \frac{k_{Bb}^2 \sigma_{Bb\to Aa}}{(1+\delta_{Bb})} \tag{2.13}$$

This expression is called *reciprocity theorem* and it holds for differential as well as total cross sections. The factors $(1+\delta_{ij})$ account for the fact that cross sections between identical particles in the entrance channel are twice those between different particles, other factors being equal.

When particles with spin are involved in the reactions, then the above equation must be modified by multiplying the density of final states by their statistical weights. Since there are $(2j_i+1)$ states of orientation available for a particle with spin j_i, we can write for unpolarized particles

$$\frac{k_{Aa}^2 (2j_A+1)(2j_a+1)\sigma_{Aa\to Bb}}{(1+\delta_{Aa})} = \frac{k_{Bb}^2 (2j_B+1)(2j_b+1)\sigma_{Bb\to Aa}}{(1+\delta_{Bb})} \tag{2.14}$$

$$\frac{\sigma_{Bb\to Aa}}{\sigma_{Aa\to Bb}} = \frac{(2j_A+1)(2j_a+1)}{(2j_B+1)(2j_b+1)} \frac{k_{Aa}^2 (1+\delta_{Bb})}{k_{Bb}^2 (1+\delta_{Aa})} \tag{2.15}$$

It follows that the cross section $\sigma_{Bb\to Aa}$ can be easily calculated, independently from any assumptions regarding the reaction mechanism, if the quantity $\sigma_{Aa\to Bb}$ is known experimentally or theoretically. Equation (2.15) is applicable to particles with rest mass as well as to photons. It must be emphasized that the symbols A, a, b, and B do not only refer to specific nuclei but, more precisely, to specific states. In other words, the reciprocity theorem connects the same nuclear levels in the forward as in the reverse reaction.

The reciprocity theorem has been tested in a number of experiments. An example is shown in Fig. 2.2. Compared are differential cross sections for the reaction pair ^{24}Mg(α,p)^{27}Al (open circles) and ^{27}Al(p,α)^{24}Mg (crosses), connecting the ground states of ^{24}Mg and ^{27}Al. Both reactions were measured at the same center-of-mass total energy and angle. The differential cross sections exhibit a complicated structure, presumably caused by overlapping broad resonances. Despite the complicated structure, it can be seen that the agreement between forward and reverse differential cross section is excellent. Such results support the conclusion that, to this accuracy, nuclear reactions are invariant under time-reversal. See also Blanke et al. (1983).

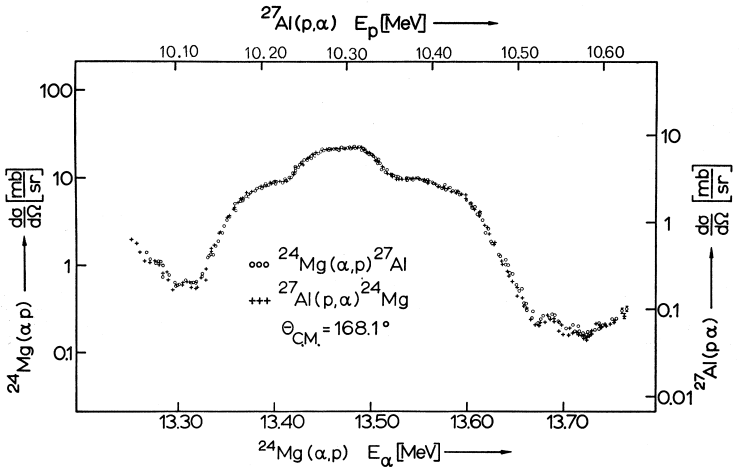

Fig. 2.2 Experimental test of the reciprocity theorem for the reaction pair ^{24}Mg(α,p)^{27}Al (open circles) and ^{27}Al(p,α)^{24}Mg (crosses), connecting the ground states of ^{24}Mg and ^{27}Al. The differential cross sections of both reactions are shown for the same total energy and detection angle in the center-of-mass system. The cross sections have also been adjusted to compensate for differences in spins. Reprinted with permission from W. von Witsch, A. Richter and P. von Brentano, Phys. Rev., Vol. 169, p. 923 (1968). Copyright (1968) by the American Physical Society.

2.3
Elastic Scattering and Method of Partial Waves

2.3.1
General Aspects

The interactions between nucleons within a nucleus and between nucleons participating in nuclear reactions have to be described using quantum mechanics. The fundamental strong interaction is very complicated and not precisely known. We know from experiments that it is of short range. Furthermore, it exhibits a part which is attractive at distances comparable to the size of a nucleus and another part which is repulsive at very short distances. Because of the complexity of this nucleon–nucleon interaction it is necessary to employ approximations. Instead of calculating all the interactions between all nucleons exactly, one frequently resorts to using effective potentials. These describe the behavior of a nucleon, or a group of nucleons (such as an α-particle), in the effective (average) field of all the other nucleons. Because of the approximate nature of this approach, the resulting effective potentials are usually tailored to specific reactions and energies and thus lack generality. The most widely used approximate potentials are called *central potentials*. They depend only on the magnitude of the radius vector, but not on its direction, that is, $V(\vec{r}) = V(r)$. Since the nuclear potential is of short range, we will consider

here only potentials that for large distances ($r \to \infty$) approach $V(r) \to 0$ faster than $1/r$.

In this section, we will initially focus on the problem of elastic scattering. The formalism is then extended to include nuclear reactions. A general treatment of nuclear scattering involves solutions of the time-dependent Schrödinger equation, that is, the scattering of wave packets. However, the most important physics aspects can be derived by considering the much simpler stationary problem of solving the time-independent Schrödinger equation. No further assumptions about the nuclear potential are made here. We will derive the general formalism which relates the observed scattering cross section to the wave function far away from the scattering center. The cross section will be expressed in terms of so-called phase shifts. In order to determine the latter quantity, knowledge of the wave function in the nuclear region is necessary. These considerations will be discussed in subsequent sections.

The scattering process is schematically shown in Fig. 2.3. Consider a beam of monoenergetic particles incident on a target along the z-direction. The value and the uncertainty of the z-component of the linear momentum are given by $p_z = \text{const}$ and $\Delta p_z = 0$, respectively. It follows immediately from the Heisenberg uncertainty principle ($\Delta p_z \Delta z \approx \hbar$) that $\Delta z \to \infty$. Hence, the incoming wave has a large extent in the z-direction, that is, the process is nearly stationary. Furthermore, we assume for the x- and y-components of the linear momentum $p_x = p_y = 0$. This implies, according to $\lambda_i = h/p_i$, that $\lambda_x = \lambda_y \to \infty$. In other words, the incoming particles are represented by a wave of very large wavelength in the x- and y-directions, that is, an incident plane wave.

The stationary scattering problem is described by the time-independent Schrödinger equation

$$\left[-\frac{\hbar^2}{2m}\nabla^2 + V(\vec{r})\right]\psi(\vec{r}) = E\psi(\vec{r}) \tag{2.16}$$

At the position of the target nucleus we cannot specify the total wave function further without assuming an explicit nuclear potential. However, far away from the scattering center, at the position of our detector, we can express the total wave function as a sum of two stationary waves: an incoming plane wave and an outgoing spherical wave. Therefore, we start for the total wave function at large distances with the ansatz

$$\psi_T(\vec{r}) = N\left[e^{i\vec{k}\cdot\vec{r}} + f(\theta)\frac{e^{ikr}}{r}\right], \qquad r \to \infty \tag{2.17}$$

The term $e^{i\vec{k}\cdot\vec{r}}$ represents a plane wave traveling in the z-direction (a free particle). The second term contains a spherical wave (e^{ikr}), a quantity $f(\theta)$ called

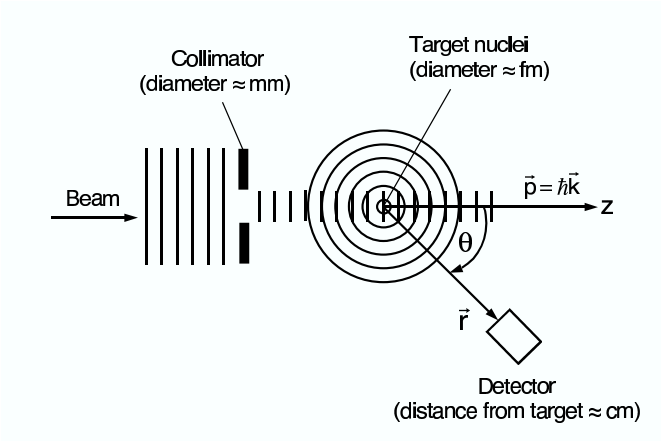

Fig. 2.3 Schematic representation of the scattering process. A plane wave is incident along the z-direction on a scattering center (target) which gives rise to an outgoing spherical wave. Note the significant differences in the dimensions of the collimator ($\approx$ mm), target nuclei ($\approx$ fm), and detector distance ($\approx$ cm), which are typical for nuclear physics experiments.

scattering amplitude, and the factor $1/r$ since the scattered intensity must obey an inverse square law; N is an overall normalization factor.

2.3.2 Relationship Between Differential Cross Section and Scattering Amplitude

The particle density (in units of inverse volume) is given by $P = \psi^*\psi$ and the current density (in units of inverse area per time) of beam particles or scattered particles with velocity v can be written as $j = vP$. For the incoming plane wave we can write

$$j_b = v_b(Ne^{-ikz})(Ne^{ikz}) = v_b N^2 \tag{2.18}$$

whereas we obtain for the scattered spherical wave

$$j_s = v_s \left[Nf^*(\theta)e^{-ikr}\frac{1}{r}\right]\left[Nf(\theta)e^{ikr}\frac{1}{r}\right] = v_s N^2 |f(\theta)|^2 \frac{1}{r^2} \tag{2.19}$$

Substitution of j_b and j_s into Eq. (2.10) yields

$$\left(\frac{d\sigma}{d\Omega}\right) = \frac{j_s r^2}{j_b} = |f(\theta)|^2 \tag{2.20}$$

since for elastic scattering we can assume that $v_b = v_s$. The important result here is that the differential cross section is equal to the square of the scattering amplitude.

2.3.3 The Free Particle

It is instructive to consider first the force-free particle. The plane wave $e^{i\vec{k}\cdot\vec{r}}$ represents a free particle of momentum $\vec{p} = \hbar\vec{k}$ and energy $E = \hbar^2k^2/(2m)$. The potential is $V(r) = 0$ and, therefore, we have $f(\theta) = 0$. If we choose the z axis along $\vec{k}$ (see Fig. 2.4), the plane wave can be written as

$$e^{i\vec{k}\cdot\vec{r}} = e^{ikr\cos\theta} = e^{ikr(z/r)} = e^{ikz} \tag{2.21}$$

which is independent of the angle ϕ. Since $\vec{L} = \vec{r} \times \vec{p}$, we only need to consider values of $m = 0$ for the magnetic quantum number. In this case, the spherical harmonics are given by (see Eq. (A.9))

$$Y_{\ell 0} = \sqrt{\frac{2\ell+1}{4\pi}}\, P_\ell(\cos\theta) \tag{2.22}$$

where $P_\ell(\cos\theta)$ is a Legendre polynomial. With the substitutions $E = p^2/(2m) = \hbar^2k^2/(2m)$ and $\rho \equiv kr$, the radial equation for the free particle can be written as (see Eq. (A.23))

$$\frac{d^2u_\ell}{d\rho^2} + \left[1 - \frac{\ell(\ell+1)}{\rho^2}\right] u_\ell = 0 \tag{2.23}$$

The solutions, $j_\ell(kr)$, are called *spherical Bessel functions* (Section A.2) and we can write for the asymptotic values

$$u_\ell^{\text{f.p.}} = (kr)j_\ell(kr) = \sin(kr - \ell\pi/2)\,, \qquad r \to \infty \tag{2.24}$$

The eigenfunctions of the free particle, $j_\ell(kr)P_\ell(\cos\theta)$, form a complete orthonormal set. Therefore, we expand the plane wave according to

$$e^{ikz} = \sum_{\ell=0}^{\infty} c_\ell j_\ell(kr) P_\ell(\cos\theta) \tag{2.25}$$

The derivation of the expansion coefficients, which is not repeated here (see, for example, Messiah 1999), yields $c_\ell = (2\ell+1)i^\ell$. Thus

$$e^{ikz} = \sum_{\ell=0}^{\infty} (2\ell+1) i^\ell j_\ell(kr) P_\ell(\cos\theta) \tag{2.26}$$

It can be seen that the plane wave with linear momentum kr has been expanded into a set of *partial waves*, each having an orbital angular momentum of $\hbar\sqrt{\ell(\ell+1)}$, an amplitude of $(2\ell+1)$, and a phase factor of i^ℓ. For very large distances appropriate for any experimental detector geometry, we find for the free particle

$$\psi_T^{\text{f.p.}} = e^{ikz} = \sum_{\ell=0}^{\infty} (2\ell+1) i^\ell \frac{\sin(kr - \ell\pi/2)}{kr}\, P_\ell(\cos\theta), \qquad r \to \infty \tag{2.27}$$

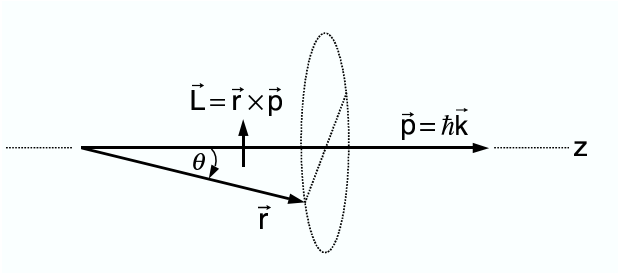

Fig. 2.4 Linear and angular momenta of the free particle. The vector $\vec{p}$ points along the z axis, while the projection of $\vec{L}$ on the z axis is zero ($m = 0$).

Using the relationship $\sin x = (i/2)(e^{-ix} - e^{ix})$ we write

$$\psi_T^{\text{f.p.}} = \frac{1}{2kr} \sum_{\ell=0}^{\infty} (2\ell + 1) i^{\ell+1} \left[e^{-i(kr - \ell\pi/2)} - e^{i(kr - \ell\pi/2)} \right] P_\ell(\cos\theta), \qquad r \to \infty \tag{2.28}$$

For the special case of s-waves ($\ell = 0$), we have $u_0^{\text{f.p.}} = \sin(kr)$ instead of Eq. (2.24) (see also Eq. (A.26)). Consequently, Eqs. (2.27) and (2.28) are not only valid for $r \to \infty$, but apply in this case to all distances.

2.3.4 Turning the Potential On

For a central potential (Section 2.3.1) with $V(r) \neq 0$ and $f(\theta) \neq 0$, only the solution to the radial equation will change. Instead of $u_\ell^{\text{f.p.}}$ we have to write u_ℓ. The two functions $u_\ell^{\text{f.p.}}$ and u_ℓ essentially differ only for small r where $V(r) \neq 0$. For large distances r we have $V(r) = 0$ and both functions must satisfy the same radial equation. We write

$$u_\ell = \sin(kr - \ell\pi/2 + \delta_\ell), \qquad r \to \infty \tag{2.29}$$

This solution can differ at most from the radial wave function of the free particle (Eq. (2.24)) by a phase shift δ_ℓ, which arises from the different r dependence in the region where $V(r) \neq 0$. Note that for s-waves ($\ell = 0$), Eq. (2.29) applies again to all distances outside the potential.

Similar to the case of the free particle (see Eq. (2.25)), we can expand the total wave function into partial waves

$$e^{ikz} + f(\theta)\frac{e^{ikr}}{r} = \sum_{\ell=0}^{\infty} b_\ell \frac{u_\ell(kr)}{kr} P_\ell(\cos\theta) \tag{2.30}$$

The expansion coefficients are given by $b_\ell = (2\ell+1)i^\ell e^{i\delta_\ell}$ (Problem 2.1). Thus

$$\begin{aligned}\psi_T &= e^{ikz} + f(\theta)\frac{e^{ikr}}{r} \\ &= \sum_{\ell=0}^{\infty}(2\ell+1)i^\ell e^{i\delta_\ell}\frac{\sin(kr-\ell\pi/2+\delta_\ell)}{kr}P_\ell(\cos\theta), \qquad r\to\infty\end{aligned} \tag{2.31}$$

Using the relation $\sin x = (i/2)(e^{-ix} - e^{ix})$ we write

$$\psi_T = \frac{1}{2kr}\sum_{\ell=0}^{\infty}(2\ell+1)i^{\ell+1}\left[e^{-i(kr-\ell\pi/2)} - e^{2i\delta_\ell}e^{i(kr-\ell\pi/2)}\right]P_\ell(\cos\theta), \qquad r\to\infty \tag{2.32}$$

Comparison to the total wave function of the free particle (Eq. (2.28)) clearly shows that the potential modifies at large distances each outgoing spherical wave by a factor of $e^{2i\delta_\ell}$ and thereby shifts each outgoing spherical wave by a phase δ_ℓ.

2.3.5
Scattering Amplitude and Elastic Scattering Cross Section

We solve first for the scattering amplitude $f(\theta)$ by writing

$$f(\theta)\frac{e^{ikr}}{r} = \psi_T - \psi_T^{\text{f.p.}} = \frac{1}{2kr}\sum_{\ell=0}^{\infty}(2\ell+1)i^{\ell+1}\left[e^{i(kr-\ell\pi/2)}\left(1-e^{2i\delta_\ell}\right)\right]P_\ell(\cos\theta) \tag{2.33}$$

Using $e^{i\pi\ell/2} = \cos(\pi\ell/2) + i\sin(\pi\ell/2) = i^\ell$ and the identity $e^{i\delta}\sin\delta \equiv (i/2)(1-e^{2i\delta})$ yields

$$f(\theta) = \frac{i}{2k}\sum_{\ell=0}^{\infty}(2\ell+1)\left(1-e^{2i\delta_\ell}\right)P_\ell(\cos\theta) = \frac{1}{k}\sum_{\ell=0}^{\infty}(2\ell+1)e^{i\delta_\ell}\sin\delta_\ell P_\ell(\cos\theta) \tag{2.34}$$

It is again apparent that the effect of the scattering potential is to shift the phase of each outgoing partial wave.

The differential elastic scattering cross section can be written as

$$\begin{aligned}\left(\frac{d\sigma}{d\Omega}\right)_{\text{el}} &= f^*(\theta)f(\theta) = \frac{1}{4k^2}\left|\sum_{\ell=0}^{\infty}(2\ell+1)\left(1-e^{2i\delta_\ell}\right)P_\ell(\cos\theta)\right|^2 \\ &= \frac{1}{k^2}\left|\sum_{\ell=0}^{\infty}(2\ell+1)\sin\delta_\ell P_\ell(\cos\theta)\right|^2\end{aligned} \tag{2.35}$$

The interference terms involving different functions $P_\ell(\cos\theta)$ generally give rise to nonisotropic angular distributions. Using the orthogonality relation for Legendre polynomials,

$$\int_{d\Omega} P_\ell(\cos\theta) P_{\ell'}(\cos\theta) d\Omega = \frac{4\pi}{2\ell+1}\delta_{\ell\ell'} \tag{2.36}$$

where $\delta_{\ell\ell'}$ denotes a Kronecker symbol, we obtain for the total elastic scattering cross section

$$\sigma_{\text{el}} = \int \left(\frac{d\sigma}{d\Omega}\right)_{\text{el}} d\Omega = \sum_{\ell=0}^{\infty} \sigma_{\text{el},\ell} \tag{2.37}$$

$$\sigma_{\text{el},\ell} = \frac{\pi}{k^2}(2\ell+1)\left|1 - e^{2i\delta_\ell}\right|^2 = \frac{4\pi}{k^2}(2\ell+1)\sin^2\delta_\ell \tag{2.38}$$

For the special case of s-waves ($\ell = 0$) we find

$$\left(\frac{d\sigma}{d\Omega}\right)_{\text{el},0} = \frac{1}{k^2}\sin^2\delta_0 \tag{2.39}$$

$$\sigma_{\text{el},0} = \frac{4\pi}{k^2}\sin^2\delta_0 \tag{2.40}$$

and the angular distribution becomes isotropic (that is, independent of θ). It follows that the cross section is entirely determined by the phase shifts δ_ℓ. It is also apparent that $\delta_\ell \to 0$ as $V(r) \to 0$ for all ℓ.

So far we assumed that at least one particle participating in the interaction is uncharged. If both nuclei are charged, then we have to replace the phase δ_ℓ for the short-range nuclear potential by $\delta_\ell + \sigma_\ell$, where σ_ℓ is the phase shift due to the long-range Coulomb potential. The Coulomb phase shift can be calculated analytically (see Eq. (D.13)). We write

$$1 - e^{2i(\delta_\ell+\sigma_\ell)} = \left(1 - e^{2i\sigma_\ell}\right) + e^{2i\sigma_\ell}\left(1 - e^{2i\delta_\ell}\right) \tag{2.41}$$

and the scattering amplitude can be expressed as

$$\begin{aligned} f(\theta) &= \frac{i}{2k}\sum_{\ell=0}^{\infty}(2\ell+1)\left[1 - e^{2i(\delta_\ell+\sigma_\ell)}\right] P_\ell(\cos\theta) \\ &= \frac{i}{2k}\sum_{\ell=0}^{\infty}(2\ell+1)\left(1 - e^{2i\sigma_\ell}\right) P_\ell(\cos\theta) \\ &\quad + \frac{i}{2k}\sum_{\ell=0}^{\infty}(2\ell+1)e^{2i\sigma_\ell}\left(1 - e^{2i\delta_\ell}\right) P_\ell(\cos\theta) \end{aligned} \tag{2.42}$$

The first term describes the scattering from a pure Coulomb field (Rutherford scattering). The second term contains the phase shifts δ_ℓ and σ_ℓ. It is obvious that the cross section will exhibit interference terms corresponding to the scattering from both the nuclear and the Coulomb potential.

2.3.6 Reaction Cross Section

We can now consider the possibility that a nuclear reaction occurs, that is, any process which is different from elastic scattering (for example, particle capture or inelastic scattering). A specific set of conditions (momentum, quantum numbers, and so on) for the outgoing particle is called a *channel*. A more precise definition of this concept will be given in later sections. Elastic scattering, inelastic scattering to a final excited state x, inelastic scattering to a different excited final state y, and so on, all correspond to different channels.

Suppose first that elastic scattering is the only possible process. In that case as many particles enter as exit from an imaginary sphere surrounding the target nucleus (Fig. 2.5a). As a result, the integral over the current density j_T, corresponding to the total wave function ψ_T for elastic scattering, is zero

$$\int_{d\Omega} j_T \, d\Omega = 0 \tag{2.43}$$

Suppose now that nonelastic processes occur as well. In that case a fraction of the incoming particles will either change kinetic energies, for example, in inelastic scattering (n,n'), or change identity, for example, in particle capture (n,γ). A number of incoming particles will disappear and, consequently, there will be a net current of particles into the sphere (Fig. 2.5b). The rate of disappearance from the elastic channel corresponds to the reaction cross section. Formally, we can write

$$\sigma_{\text{re}} = \frac{r^2}{j_b} \int_{d\Omega} j_T \, d\Omega \tag{2.44}$$

Recall that the wave function ψ_T, corresponding to the current density j_T, represents the wave function for elastic scattering only. In the following, an expression is derived which relates the reaction cross section to the phase shifts. We start from the quantum mechanical expression for the current density (Messiah 1999),

$$j = \frac{\hbar}{2mi} \left(\psi^* \frac{\partial \psi}{\partial r} - \frac{\partial \psi^*}{\partial r} \psi \right) \tag{2.45}$$

From this expression we find for the incoming plane wave e^{ikz}

$$j_b = \frac{\hbar}{2mi} \left[e^{-ikz}(e^{ikz} ik) - e^{-ikz}(-ik) e^{ikz} \right] = \frac{\hbar k}{m} \tag{2.46}$$

Substitution of the total elastic scattering wave function ψ_T (see Eq. (2.32)) into

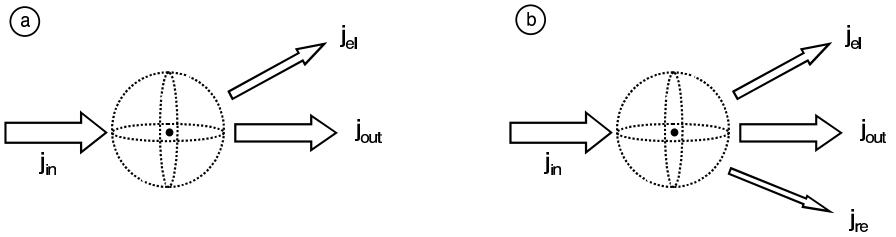

Fig. 2.5 Representation of the current density if (a) scattering is the only possible process, and (b) both elastic and nonelastic processes occur. In part (a) the same number of particles enter and exit from an imaginary sphere surrounding the target nucleus and the integral over the total current density is zero. In part (b) a number of incoming particles disappear because of reactions and thus there is a net current of particles into the sphere.

Eq. (2.45) yields, after some algebra,

$$j_T = \frac{\hbar}{4mkr^2}\left\{\left|\sum_{\ell=0}^{\infty}(2\ell+1)i^{\ell+1}e^{i\ell\pi/2}P_\ell(\cos\theta)\right|^2 - \left|\sum_{\ell=0}^{\infty}(2\ell+1)i^{\ell+1}e^{2i\delta_\ell}e^{-i\ell\pi/2}P_\ell(\cos\theta)\right|^2\right\} \tag{2.47}$$

With the orthogonality relation for Legendre polynomials (see Eq. (2.36)), one finds

$$\sigma_{\mathrm{re}} = \sum_{\ell=0}^{\infty}\sigma_{\mathrm{re},\ell} \tag{2.48}$$

$$\sigma_{\mathrm{re},\ell} = \frac{\pi}{k^2}(2\ell+1)\left(1-\left|e^{2i\delta_\ell}\right|^2\right) \tag{2.49}$$

We require $|e^{2i\delta_\ell}|^2 \leq 1$ since otherwise σ_{re} becomes negative. In general, the phase shift δ_ℓ will be a complex number, that is, $\delta_\ell = \delta_{\ell_1} + i\delta_{\ell_2}$. For the special case that δ_ℓ is real, one finds $|e^{2i\delta_\ell}|^2 = 1$. In other words, reactions cannot occur and elastic scattering is the only possible process. The allowed range of values for $\sigma_{\mathrm{re},\ell}$ and $\sigma_{\mathrm{el},\ell}$ is represented by the shaded region in Fig. 2.6. Recall that the expression for the elastic scattering cross section (see Eq. (2.38)) holds only for uncharged particles. The maximum elastic scattering cross section occurs at $e^{2i\delta_\ell} = -1$, yielding

$$\sigma_{\mathrm{el},\ell}^{\max} = \frac{4\pi}{k^2}(2\ell+1) \qquad \text{and} \qquad \sigma_{\mathrm{re},\ell} = 0 \tag{2.50}$$

The maximum reaction cross section is obtained for $e^{2i\delta_\ell} = 0$, leading to

$$\sigma_{\mathrm{re},\ell}^{\max} = \sigma_{\mathrm{el},\ell} = \frac{\pi}{k^2}(2\ell+1) \tag{2.51}$$

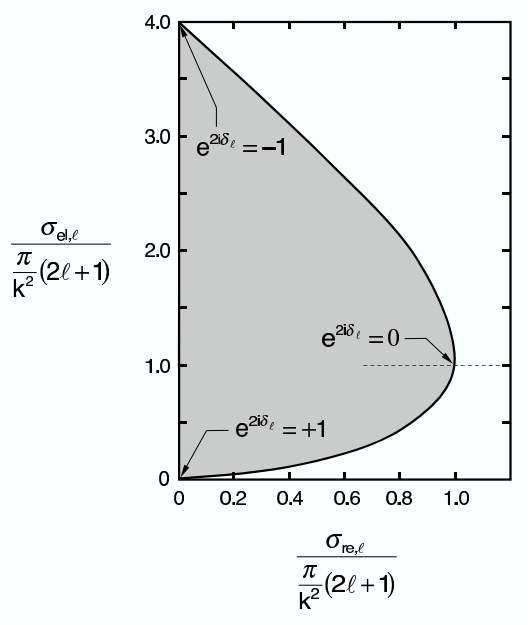

Fig. 2.6 Upper and lower limit of elastic scattering cross section for a given reaction cross section. Values inside the shaded region are allowed, while those outside the shaded region are impossible. The quantity $e^{2i\delta_\ell}$ is real for all points located on the solid curve.

It follows that elastic scattering may occur without any reactions taking place, but reactions can never occur without elastic scattering being present. When the reaction cross section is at maximum, its value is equal to the elastic scattering cross section.

Traditionally, the theory of scattering has been applied in order to study the nature of the nuclear potential. Usually, the differential cross section $d\sigma/d\Omega$ is given by experiment and it is desired to find the corresponding potential $V(r)$. The experimental phase shifts δ_ℓ are obtained by fitting the cross section formula to experimental angular distribution data, provided that a satisfactory fit is achieved by means of a small number of terms in the partial wave expansion. This procedure is repeated for several values of the incident energy. One then attempts to find a potential $V(r)$, which reproduces the observed phase shifts, by solving the Schrödinger equation numerically for each value of ℓ.

2.4 Scattering by Simple Potentials

The cross section is determined by the phase shifts. The latter can be obtained from the wave function in the nuclear region that is generated by an explicit nuclear potential. In this section, we will consider the case of s-wave ($\ell = 0$) scattering of neutral and spinless particles. Two simple potentials will be discussed explicitly: (i) an attractive square-well potential, and (ii) an attractive square-well plus square-barrier potential. Although very simple, these models contain qualitatively most of the physics that will be encountered later in the discussion of far more complex situations. We will specifically calculate the phase shifts δ_0 and the intensity of the wave function in the region of the potential by solving the radial Schrödinger equation. It will be seen how the properties of the potential determine the phase shift and the wave function intensity.

2.4.1 Square-Well Potential

The potential is displayed in Fig. 2.7. For $\ell = 0$ the radial equation becomes (Appendix A.1)

$$\frac{d^2u}{dr^2} + \frac{2m}{\hbar^2}[E - V(r)]u = 0 \tag{2.52}$$

For a constant potential, $V(r) = \text{const}$, we obtain with $\hat{k}^2 = (2m/\hbar^2)(E - V)$ the radial equation

$$\frac{d^2u}{dr^2} + \hat{k}^2 u = 0 \tag{2.53}$$

The general solution in terms of complex exponentials is given by

$$u = \alpha e^{i\hat{k}r} + \beta e^{-i\hat{k}r} \tag{2.54}$$

We will consider the two regions $r < R_0$ and $r > R_0$ separately. For $r < R_0$ we have $E - V > 0$ and, therefore,

$$\begin{aligned} u_{\text{in}} &= A' e^{iKr} + B' e^{-iKr}, \qquad K^2 = \frac{2m}{\hbar^2}(E + V_0) \\ &= A'[\cos(Kr) + i\sin(Kr)] + B'[\cos(Kr) - i\sin(Kr)] \end{aligned} \tag{2.55}$$

At the boundary we require $u_{\text{in}}(0) = 0$, otherwise the radial wave function $u(r)/r$ will diverge at $r = 0$. It follows immediately that $u_{\text{in}}(0) = A' + B' = 0$ and the cosine terms in Eq. (2.55) disappear. Hence

$$u_{\text{in}} = A' i \sin(Kr) - A'[-i\sin(Kr)] = 2iA' \sin(Kr) = A\sin(Kr) \tag{2.56}$$

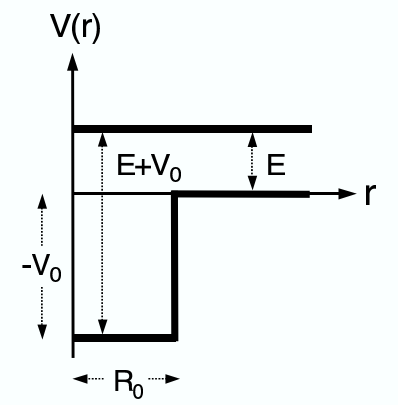

Fig. 2.7 Three-dimensional square-well potential of radius R_0 and potential depth V_0. The horizontal line indicates the total particle energy E. For the calculation of the transmission coefficient, it is necessary to consider a one-dimensional potential step that extends from $-\infty$ to $+\infty$. See the text.

where we used the definition $A \equiv 2iA'$. In the region $r > R_0$, one finds again $E - V > 0$, and the general solution is given by

$$\begin{aligned} u_{\text{out}} &= C' e^{ikr} + D' e^{-ikr}, \qquad k^2 = \frac{2m}{\hbar^2} E \\ &= C'[\cos(kr) + i \sin(kr)] + D'[\cos(kr) - i \sin(kr)] \\ &= i[C' - D'] \sin(kr) + [C' + D'] \cos(kr) = C'' \sin(kr) + D'' \cos(kr) \end{aligned} \tag{2.57}$$

It is convenient to rewrite this expression. The sum of $\sin x$ and $\cos x$ gives again a sine function which is shifted along the x-axis. Using $C'' = C \cos \delta_0$ and $D'' = C \sin \delta_0$ we can formally write

$$u_{\text{out}} = C\,[\sin(kr) \cos \delta_0 + \cos(kr) \sin \delta_0] \tag{2.58}$$

With $\sin(x \pm y) = \sin x \cos y \pm \cos x \sin y$ one finds

$$u_{\text{out}} = C \sin(kr + \delta_0) \tag{2.59}$$

The solutions u_{in} (see Eq. (2.56)) and u_{out} (see Eq. (2.59)) will be used below.

Transmission probability

We are interested in the transmission probability from the outer to the inner region. It is convenient to start from the wave function solutions in terms of complex exponentials (see Eqs. (2.55) and (2.57)). It should be pointed out that for real potentials, the transmission probability is only defined for the one-dimensional case (see, for example, Messiah 1999). Instead of considering the

three-dimensional potential shown in Fig. 2.7, we will assume that the particles are incident from the right-hand side, that a one-dimensional potential steps down at a distance of $x = R_0$ by an amount of V_0, and that the potential step extends to $-\infty$. We obtain for the one-dimensional radial wave functions

$$u_{\text{in}} = A' e^{iKx} + B' e^{-iKx} \tag{2.60}$$

$$u_{\text{out}} = C' e^{ikx} + D' e^{-ikx} \tag{2.61}$$

Although we do not have to consider the time-dependent Schrödinger equation here, it is instructive to investigate the full time-dependent solution, which is obtained by multiplying the complex exponentials by the factor $e^{-i\omega t}$, with $\omega = E/\hbar$. It can easily be seen, for example, that the second term of u_{in} corresponds to a plane wave that propagates into the negative x direction. The first and second terms of u_{out} correspond to plane waves reflected from the boundary at R_0 and moving toward R_0, respectively. We are interested in the scattering process. The particle density of incident projectiles, for example, is given by $|D' e^{-ikx}|^2 = |D'|^2$. The current density (or flux) of incident particles is given by the product of particle density and velocity in the outer region, $j_{\text{inc}} = v_{\text{out}}|D'|^2$ (Section 2.3.2). Similarly, one finds for the transmitted or reflected particle flux $j_{\text{trans}} = v_{\text{in}}|B'|^2$ or $j_{\text{refl}} = v_{\text{out}}|C'|^2$, respectively. It follows for the probability that an individual particle will be transmitted from the outer to the inner region

$$\hat{T} = \frac{j_{\text{trans}}}{j_{\text{inc}}} = \frac{v_{\text{in}}|B'|^2}{v_{\text{out}}|D'|^2} = \frac{K|B'|^2}{k|D'|^2} \tag{2.62}$$

The quantity $\hat{T}$ is called the *transmission coefficient*.

The continuity condition requires that the wave functions and their derivatives are continuous at the boundary $x = R_0$,

$$(u_{\text{in}})_{R_0} = (u_{\text{out}})_{R_0} \tag{2.63}$$

$$\left(\frac{du_{\text{in}}}{dx}\right)_{R_0} = \left(\frac{du_{\text{out}}}{dx}\right)_{R_0} \tag{2.64}$$

We obtain

$$A' e^{iKR_0} + B' e^{-iKR_0} = C' e^{ikR_0} + D' e^{-ikR_0} \tag{2.65}$$

$$\frac{K}{k}\left(A' e^{iKR_0} - B' e^{-iKR_0}\right) = \left(C' e^{ikR_0} - D' e^{-ikR_0}\right) \tag{2.66}$$

Setting $A' = 0$, since there is no plane wave approaching the boundary R_0 from the left-hand side, and eliminating C' yields

$$\frac{K}{k}\left(-B' e^{-iKR_0}\right) = B' e^{-iKR_0} - 2D' e^{-ikR_0} \qquad \text{or} \qquad \frac{B'}{D'} = 2\frac{e^{-ikR_0}}{e^{-iKR_0}}\frac{k}{K+k} \tag{2.67}$$

For the transmission coefficient we find with Eqs. (2.62) and (2.67)

$$\hat{T} = \frac{K}{k}\frac{|B'|^2}{|D'|^2} = 4\frac{kK}{(K+k)^2} = 4\frac{\frac{2m}{\hbar^2}\sqrt{(E+V_0)E}}{\left[\sqrt{\frac{2m}{\hbar^2}(E+V_0)} + \sqrt{\frac{2m}{\hbar^2}E}\right]^2} \tag{2.68}$$

We will use this result later in connection with the continuum theory of nuclear reactions (Section 2.6).

Phase shift and resonance phenomenon

The quantity $\hat{T}$ describes the transmission probability from the right- to the left-hand side in Fig. 2.7. We have considered so far only the amplitude ratio of two waves: one approaching the boundary R_0 from the right, the other one receding from R_0 to the left. We will now consider the full radial wave function solution for the three-dimensional case. We start from Eqs. (2.56) and (2.59),

$$u_{\text{in}} = A\sin(Kr) \tag{2.69}$$

$$u_{\text{out}} = C\sin(kr + \delta_0) \tag{2.70}$$

From the continuity condition (see Eqs. (2.63) and (2.64)) one finds

$$A\sin(KR_0) = C\sin(kR_0 + \delta_0) \tag{2.71}$$

$$AK\cos(KR_0) = Ck\cos(kR_0 + \delta_0) \tag{2.72}$$

First, we divide both equations to solve for the phase shift δ_0. The result is

$$\frac{1}{K}\tan(KR_0) = \frac{1}{k}\tan(kR_0 + \delta_0) \tag{2.73}$$

$$\delta_0 = -kR_0 + \arctan\left[\frac{k}{K}\tan(KR_0)\right] \tag{2.74}$$

This expression can be rewritten in terms of the total energy as

$$\delta_0 = -\frac{\sqrt{2mE}}{\hbar}R_0 + \arctan\left[\sqrt{\frac{E}{E+V_0}}\tan\left(\frac{\sqrt{2m(E+V_0)}}{\hbar}R_0\right)\right] \tag{2.75}$$

It can be seen that the phase shift is determined by the properties of the potential (R_0,V_0) and the properties of the particle (E,m). For $V_0 \to 0$ one finds $\delta_0 \to 0$, as already pointed out above. The cross section can be calculated simply from the phase shift (see Eq. (2.40)). Second, one can solve for $|A|^2/|C|^2$, that is, the ratio of wave function intensities in the interior ($r < R_0$) and exterior regions ($r > R_0$). By squaring and adding Eqs. (2.71) and (2.72) we obtain

$$\frac{|A|^2}{|C|^2} = \frac{k^2}{k^2 + [K^2 - k^2]\cos^2(KR_0)} = \frac{E}{E + V_0\cos^2\left(\frac{\sqrt{2m(E+V_0)}}{\hbar}R_0\right)} \tag{2.76}$$

where the identity $\sin^2(kr+\delta) + \cos^2(kr+\delta) = 1$ has been used.

Plots of $|A|^2/|C|^2$ and δ_0 versus E for the scattering of a neutron by a square-well potential are shown in Fig. 2.8. A potential depth of V_0 = 100 MeV and a potential radius of R_0 = 3 fm are assumed. The quantity $|A|^2/|C|^2$ measures the relative intensity of the wave function in the interior region $r < R_0$. It is apparent that $|A|^2/|C|^2$ oscillates between extreme values. This remarkable behavior is referred to as *resonance phenomenon*. At certain discrete energies E_i (resonance energies) the probability for finding the particle inside the boundary $r < R_0$ is at maximum. It can also be seen that each resonance shifts the phase δ_0 by some amount. The resonances occur at energies at which $\cos^2(KR_0) = 0$ in Eq. (2.76), that is, $KR_0 = (n + 1/2)\pi$. Hence

$$K = \frac{\left(n + \frac{1}{2}\right)\pi}{R_0} = \frac{2\pi}{\lambda_{\text{in}}} \tag{2.77}$$

$$\lambda_{\text{in}} = \frac{2R_0}{\left(n + \frac{1}{2}\right)} = \frac{R_0}{\left(\frac{n}{2} + \frac{1}{4}\right)} \tag{2.78}$$

with λ_{in} the wavelength in the interior region. Since $(n/2 + 1/4) = \frac{1}{4}, \frac{3}{4}, \frac{5}{4}, \ldots$ it follows that resonances occur when precisely $(n/2 + 1/4)$ wavelengths fit into the interior region. At those wavelengths, the derivative of the interior wave function (a sine function; see Eq. (2.69)) at the radius R_0 is zero. As can be seen in Fig. 2.9, n also corresponds to the number of wave function nodes in the region $r < R_0$. For the resonance energies we obtain from Eq. (2.77)

$$E_n = \frac{\hbar^2}{2m}\frac{\pi^2}{R_0^2}\left(n + \frac{1}{2}\right)^2 - V_0 \tag{2.79}$$

In the above example of neutron scattering by a square-well potential of depth V_0 = 100 MeV and radius R_0 = 3 fm, one has $(\hbar\pi)^2/(2mR_0^2)$ = 22.648 MeV. We obtain

$$E_2 = 41.5\,\text{MeV}, \qquad E_3 = 177.4\,\text{MeV}, \qquad E_4 = 358.6\,\text{MeV}, \ldots \tag{2.80}$$

No physical solution exists for n = 0 or 1, that is, for the potential depth chosen it is not possible to match the interior and exterior wave functions by fitting either 1/4 or 3/4 wavelengths into the region $r < R_0$. In other words, there are no solutions with either no node or only one node in the interior region.

The results obtained from the above formalism are illustrated qualitatively in Fig. 2.10 showing radial wave functions for different depths of an attractive square-well potential. The bombarding energy is low (that is, the wavelength is large compared to R_0) and held constant. In part (a) the potential depth is zero (free particle) and the wave function is given by a sine function. In part (b), the potential depth increases and, therefore, the wavelength in the

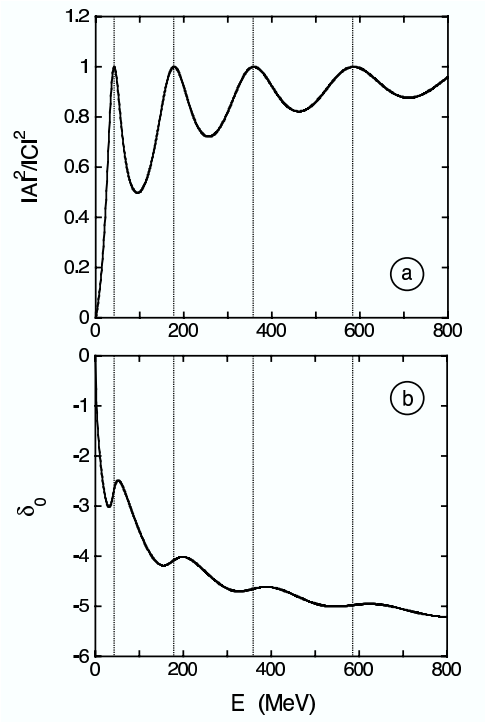

Fig. 2.8 (a) Ratio of wave function intensities in the interior ($r < R_0$) and exterior ($r > R_0$) region, $|A|^2/|C|^2$, and (b) phase shift δ_0 versus total energy E for the scattering of neutrons ($2m/\hbar^2 = 0.0484\ \mathrm{MeV}^{-1}\mathrm{fm}^{-2}$) by a square-well potential (Fig. 2.7). For the potential depth and the radius, values of V_0 = 100 MeV and R_0 = 3 fm, respectively, are assumed. The curves show the resonance phenomenon.

interior decreases according to

$$\frac{\lambda_{\mathrm{in}}}{2\pi} = \frac{1}{K} = \frac{1}{\sqrt{(2m/\hbar^2)(E+V_0)}}, \qquad \lambda_{\mathrm{in}} = \frac{h}{\sqrt{2m(E+V_0)}} \tag{2.81}$$

The values and derivatives of the inside and outside wave functions can only be matched by shifting the outside solution inward. This is the physical meaning of a phase shift. If the potential depth is increased further, the wavelength in the interior becomes smaller and the exterior wave must shift inward, until exactly $1/4$ wavelength fit into the interior region. When this happens, the derivative of the wave function at R_0 becomes zero corresponding to a maximum amplitude inside the potential region. The system is in resonance as shown in part (c). A further increase in the potential depth results in: a decreasing amplitude in the interior (part d); a minimum interior amplitude because of poor

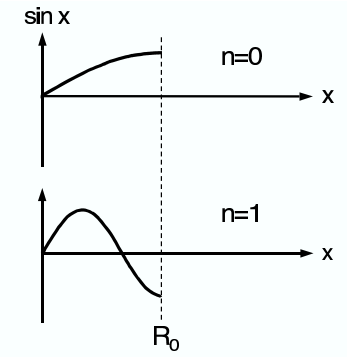

Fig. 2.9 Two simplest solutions for the radial wave function inside the square-well potential. Both solutions give rise to a resonance since the derivative of the wave function at the potential radius R_0 is zero. The solutions are characterized by the number of wave function nodes n in the interior region ($r < R_0$). They are shown here for illustrative purposes. Note that neither of these functions represent physical solutions for the conditions adopted in Fig. 2.8.

wave function matching conditions (part e); and the appearance of the first node in the interior region (part f).

A plot of $|A|^2/|C|^2$ versus potential depth V_0 is shown in Fig. 2.11. A total energy of E = 1 MeV and a potential radius of R_0 = 3 fm are assumed. Solving Eq. (2.79) for the potential depth V_0 yields

$$V_{0,n} = \frac{\hbar^2}{2m}\frac{\pi^2}{R_0^2}\left(n+\frac{1}{2}\right)^2 - E \tag{2.82}$$

Thus, we expect resonances to occur at $V_{0,0}$ = 4.7 MeV, $V_{0,1}$ = 49.9 MeV, $V_{0,2}$ = 140.5 MeV, $V_{0,3}$ = 276.4 MeV, $V_{0,4}$ = 457.6 MeV, and so on (with n = 0, 1, 2, 3, 4 nodes in the interior region, respectively), in agreement with the results displayed in Fig. 2.11.

2.4.2 Square-Barrier Potential

In the following we will again consider the simple case of s-wave ($\ell = 0$) scattering. In addition to an attractive square well, the potential displays a repulsive square barrier. This is a simple model for a nuclear reaction if a barrier is present. For example, the Coulomb potential provides a barrier in reactions involving charged particles. By solving the Schrödinger equation explicitly, we will find the probability for transmission through the potential barrier and the intensity of the wave in the interior region. The potential is displayed in Fig. 2.12. We will consider the three regions I, II, III separately. In each region, the potential is constant and, assuming $\ell = 0$, we again obtain

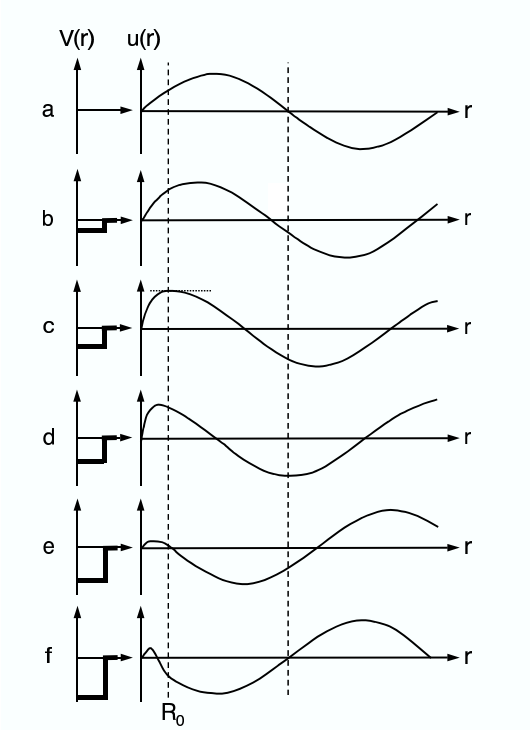

Fig. 2.10 Square-well potential (left) and corresponding radial wave function solutions (right) for different potential depths. For a given depth of the potential, the values and derivatives of the inside and outside wave functions must be matched by shifting the outside solution. The phase shift is a measure for this displacement. In part (c) the derivative of the wave function at R_0 is zero and the system is in resonance.

with $\hat{k}^2 = (2m/\hbar^2)(E - V)$ the radial equation (Appendix A.1)

$$\frac{d^2u}{dr^2} + \hat{k}^2 u = 0 \tag{2.83}$$

For region I, we have $E - V > 0$ and, therefore,

$$\begin{aligned} u_{\mathrm{I}} &= Ae^{iKr} + Be^{-iKr}, \qquad K^2 = \frac{2m}{\hbar^2}(E + V_0) \\ &= A' \sin(Kr) \end{aligned} \tag{2.84}$$

The solution is the same as the one obtained in the study of the square-well potential (see Eq. (2.56)). In region II, we have $E - V < 0$ and k_{II} becomes

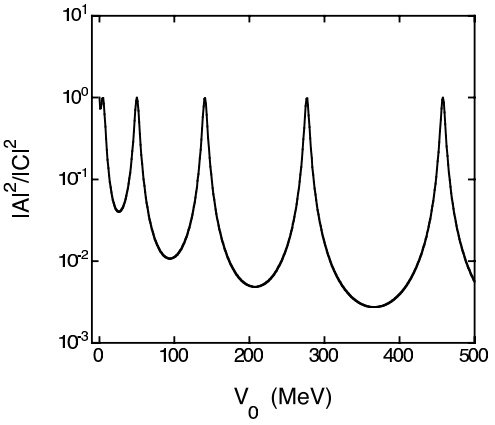

Fig. 2.11 Plot of $|A|^2/|C|^2$ versus potential depth V_0 for the scattering of neutrons by a square-well potential. For the total energy and the potential radius, values of E = 1 MeV and R_0 = 3 fm are assumed. The maxima show resonances corresponding to n = 0, 1, 2, 3, and 4 radial wave function nodes in the interior region.

imaginary. The solution can be written in terms of real exponentials as

$$u_{\rm II} = Ce^{ik_{\rm II}r} + De^{-ik_{\rm II}r}, \qquad k_{\rm II}^2 = \frac{2m}{\hbar^2}(E - V_1) = i^2\frac{2m}{\hbar^2}(V_1 - E) \equiv i^2\kappa^2$$
$$= Ce^{-\kappa r} + De^{\kappa r} \tag{2.85}$$

In region III, we have again $E - V > 0$, and the general solution is given by

$$u_{\rm III} = Fe^{ikr} + Ge^{-ikr}, \qquad k^2 = \frac{2m}{\hbar^2}E$$
$$= F' \sin(kr + \delta_0) \tag{2.86}$$

The solution is the same as the one obtained in the study of the square-well potential (see Eq. (2.59)).

Transmission through the barrier

First, we are interested in the transmission probability through the potential barrier. It is convenient to start from the wave function solutions in terms of complex exponentials (see Eqs. (2.84)–(2.86)). We must again perform the calculation for the one-dimensional case. Instead of considering the three-dimensional potential shown in Fig. 2.12, we will assume that the particles are incident from the right-hand side, that they encounter at a distance of $x = R_1$ a one-dimensional step barrier of height V_1, that at a distance of $x = R_0$ the potential steps down to $-V_0$, and that this potential continues to $-\infty$. We

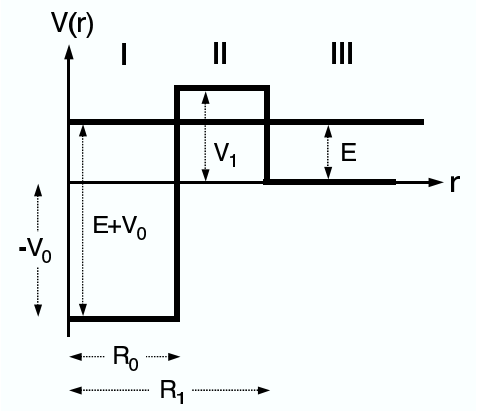

Fig. 2.12 Three-dimensional square-well potential of radius R_0 and potential depth V_0 and a repulsive square-barrier potential of thickness $R_1 - R_0$ and height V_1. The total particle energy (horizontal line) is smaller than the barrier height, $E < V_1$. For the calculation of the transmission coefficient, it is necessary to consider a one-dimensional potential that extends from $-\infty$ to $+\infty$. See the text.

obtain for the one-dimensional radial wave functions

$$u_{\mathrm{I}} = Ae^{iKx} + Be^{-iKx} \tag{2.87}$$

$$u_{\mathrm{II}} = Ce^{-\kappa x} + De^{\kappa x} \tag{2.88}$$

$$u_{\mathrm{III}} = Fe^{ikx} + Ge^{-ikx} \tag{2.89}$$

The second term of u_{I} corresponds to a plane wave that propagates into the negative x direction, whereas the first and second terms of u_{III} correspond to plane waves reflected from the barrier and moving toward the barrier, respectively. The transmission coefficient is then given by $\hat{T} = j_{\mathrm{trans}}/j_{\mathrm{inc}} = (K|B|^2)/(k|G|^2)$ (see Eq. (2.62)).

The continuity condition (see Eqs. (2.63) and (2.64)) requires that the wave functions and their derivatives are continuous at the boundaries $x = R_0$ and $x = R_1$

$$(u_{\mathrm{I}})_{R_0} = (u_{\mathrm{II}})_{R_0} \qquad (u_{\mathrm{II}})_{R_1} = (u_{\mathrm{III}})_{R_1} \tag{2.90}$$

$$\left(\frac{du_{\mathrm{I}}}{dx}\right)_{R_0} = \left(\frac{du_{\mathrm{II}}}{dx}\right)_{R_0} \qquad \left(\frac{du_{\mathrm{II}}}{dx}\right)_{R_1} = \left(\frac{du_{\mathrm{III}}}{dx}\right)_{R_1} \tag{2.91}$$

We obtain specifically

$$Ae^{iKR_0} + Be^{-iKR_0} = Ce^{-\kappa R_0} + De^{\kappa R_0} \tag{2.92}$$

$$i\frac{K}{\kappa}\left(Ae^{iKR_0} - Be^{-iKR_0}\right) = -Ce^{-\kappa R_0} + De^{\kappa R_0} \tag{2.93}$$

$$Ce^{-\kappa R_1} + De^{\kappa R_1} = Fe^{ikR_1} + Ge^{-ikR_1} \tag{2.94}$$

$$-Ce^{-\kappa R_1} + De^{\kappa R_1} = i\frac{k}{\kappa}\left(Fe^{ikR_1} - Ge^{-ikR_1}\right) \tag{2.95}$$

Adding and subtracting pairs of equations yields

$$A\left(1 + i\frac{K}{\kappa}\right)e^{iKR_0} + B\left(1 - i\frac{K}{\kappa}\right)e^{-iKR_0} = 2De^{\kappa R_0} \tag{2.96}$$

$$A\left(1 - i\frac{K}{\kappa}\right)e^{iKR_0} + B\left(1 + i\frac{K}{\kappa}\right)e^{-iKR_0} = 2Ce^{-\kappa R_0} \tag{2.97}$$

$$2De^{\kappa R_1} = F\left(1 + i\frac{k}{\kappa}\right)e^{ikR_1} + G\left(1 - i\frac{k}{\kappa}\right)e^{-ikR_1} \tag{2.98}$$

$$2Ce^{-\kappa R_1} = F\left(1 - i\frac{k}{\kappa}\right)e^{ikR_1} + G\left(1 + i\frac{k}{\kappa}\right)e^{-ikR_1} \tag{2.99}$$

Elimination of the coefficients C and D, and using the definitions $\alpha \equiv 1 + iK/\kappa$ and $\beta \equiv 1 + ik/\kappa$ gives

$$A\alpha e^{iKR_0} + B\alpha^* e^{-iKR_0} = e^{-\kappa(R_1 - R_0)}\left(F\beta e^{ikR_1} + G\beta^* e^{-ikR_1}\right) \tag{2.100}$$

$$A\alpha^* e^{iKR_0} + B\alpha e^{-iKR_0} = e^{\kappa(R_1 - R_0)}\left(F\beta^* e^{ikR_1} + G\beta e^{-ikR_1}\right) \tag{2.101}$$

Of interest is the transmission coefficient $\hat{T}$ of a wave incident from the right-hand side on the potential barrier. Since there is no wave approaching the barrier from the left-hand side, we set $A = 0$. We can also eliminate F and obtain

$$B\left[\alpha^*\beta^* e^{\kappa\Delta} - \alpha\beta e^{-\kappa\Delta}\right] = G\left[(\beta^*)^2 - \beta^2\right]e^{-i(kR_1 - KR_0)} = -2i\frac{k}{\kappa}Ge^{-i(kR_1 - KR_0)} \tag{2.102}$$

where we used $\Delta \equiv R_1 - R_0$. The transmission coefficient is then given by

$$\hat{T} = \frac{K}{k}\frac{|B|^2}{|G|^2} = \frac{4Kk/\kappa^2}{\left|\alpha^*\beta^* e^{\kappa\Delta} - \alpha\beta e^{-\kappa\Delta}\right|^2} \tag{2.103}$$

Using the relation $\sinh^2 z = (1/4)(e^{2z} + e^{-2z}) - 1/2$ yields after some algebra

$$\hat{T} = \frac{Kk}{[K + k]^2 + [\kappa^2 + K^2 + k^2 + K^2k^2/\kappa^2]\sinh^2(\kappa\Delta)} \tag{2.104}$$

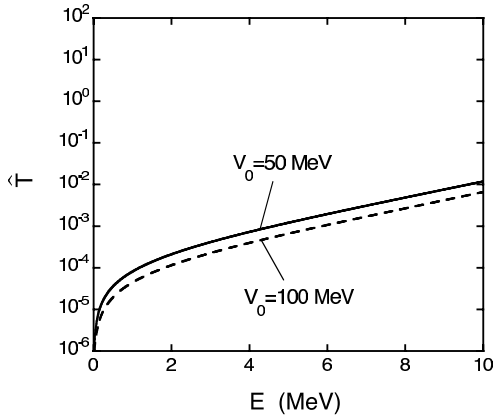

Fig. 2.13 Transmission coefficient $\hat{T}$ versus energy E for the scattering of neutrons by the square-barrier potential shown in Fig. 2.12. The potential properties are (a) V_0 = 100 MeV, V_1 = 10 MeV, R_0 = 3 fm, R_1 = 8 fm, and (b) V_0 = 50 MeV, V_1 = 10 MeV, R_0 = 3 fm, R_1 = 8 fm. The drastic drop of the transmission coefficient at small energies is apparent.

In terms of energies one finds explicitly

$$\frac{1}{\hat{T}} = \frac{1}{\sqrt{E(E+V_0)}} \left\{ \left[2E + V_0 + 2\sqrt{E(E+V_0)} \right] + \left[E + V_0 + V_1 + \frac{E(E+V_0)}{V_1 - E} \right] \sinh^2 \left[\sqrt{(2m/\hbar^2)(V_1 - E)}\, \Delta \right] \right\} \quad (2.105)$$

This result is remarkable since it shows that a particle approaching the potential barrier from the right-hand side can reach the left-hand side even if its total energy is less than the barrier height. This is referred to as the *tunnel effect* and is of central importance for charged-particle reactions in stars, as will be shown in Chapter 3.

Plots of $\hat{T}$ versus E for the scattering of neutrons are shown in Fig. 2.13. The values used are (a) V_0 = 100 MeV, V_1 = 10 MeV, R_0 = 3 fm, R_1 = 8 fm, and (b) V_0 = 50 MeV, V_1 = 10 MeV, R_0 = 3 fm, R_1 = 8 fm. It can be seen that the transmission coefficient drops rapidly with decreasing energy E. It is also apparent from the absolute magnitude of $\hat{T}$ that the intensity of the wave receding from the barrier to the left-hand side is much smaller compared to the intensity of the wave approaching the barrier from the right-hand side.

Frequently, the case of a low bombarding energy or a thick barrier is of interest,

$$\kappa\Delta = \frac{\sqrt{2m(V_1 - E)}}{\hbar}(R_1 - R_0) \gg 1 \quad (2.106)$$

In this case we can approximate the denominator in Eq. (2.103) by

$$\left|\alpha^*\beta^* e^{\kappa\Delta} - \alpha\beta e^{-\kappa\Delta}\right|^2 \approx \left|\alpha^*\beta^* e^{\kappa\Delta}\right|^2 \tag{2.107}$$

After some algebra we obtain

$$\hat{T} \approx 4\frac{\sqrt{E(E+V_0)}(V_1-E)}{V_1(V_0+V_1)}\, e^{-2\kappa(R_1-R_0)} \tag{2.108}$$

The energy dependence of the transmission coefficient is entirely dominated by the exponential factor. For physically reasonable values of E, V_0, and V_1, the coefficient in front of the exponential is of the order of unity. Hence we find

$$\hat{T} \approx e^{-(2/\hbar)\sqrt{2m(V_1-E)}(R_1-R_0)} \tag{2.109}$$

This important result, which strictly applies to the s-wave ($\ell = 0$) scattering of neutral particles, will be used later in connection with the transmission through the Coulomb barrier (Section 2.4.3).

Resonances

In the previous section, we derived the transmission probability for a one-dimensional square-barrier potential. The full radial wave function solution for the three-dimensional case will now be considered. It is interesting to have a closer look at the situation. For region I we expect again a resonance phenomenon due to good wave function matching conditions. For region III we expect again a phase shift in order to match the solutions smoothly at $r = R_1$. The barrier in region II provides an extra complication. Here, the wave function u_{II} is given by real exponentials and, depending on the relative magnitude of the coefficients C and D, may represent a decreasing, an increasing, or a more complicated function of the radius r.

As we did in the study of the square-well potential, we will calculate the energy dependence of the phase shift δ_0 and of $|A'|^2$, the intensity of the wave in the interior region $r < R_0$. We start from the wave function solutions (see Eqs. (2.84)–(2.86))

$$u_{\mathrm{I}} = A' \sin(Kr) \tag{2.110}$$

$$u_{\mathrm{II}} = Ce^{-\kappa r} + De^{\kappa r} \tag{2.111}$$

$$u_{\mathrm{III}} = F' \sin(kr + \delta_0) \tag{2.112}$$

and apply again the continuity condition (see Eqs. (2.63) and (2.64)) to the boundaries $r = R_0$ and $r = R_1$. It follows that

$$A' \sin(KR_0) = Ce^{-\kappa R_0} + De^{\kappa R_0} \tag{2.113}$$

$$A' \frac{K}{\kappa} \cos(KR_0) = -Ce^{-\kappa R_0} + De^{\kappa R_0} \tag{2.114}$$

$$Ce^{-\kappa R_1} + De^{\kappa R_1} = F' \sin(kR_1 + \delta_0) \tag{2.115}$$

$$-Ce^{-\kappa R_1} + De^{\kappa R_1} = F' \frac{k}{\kappa} \cos(kR_1 + \delta_0) \tag{2.116}$$

Solving for δ_0 by eliminating A', F', C, and D yields

$$\delta_0 = -kR_1 + \arctan\left[\frac{k}{\kappa} \frac{\sin(KR_0)\left(e^{-\kappa\Delta} + e^{\kappa\Delta}\right) + \frac{K}{\kappa}\cos(KR_0)\left(e^{\kappa\Delta} - e^{-\kappa\Delta}\right)}{\sin\left(KR_0\right)\left(e^{\kappa\Delta} - e^{-\kappa\Delta}\right) + \frac{K}{\kappa}\cos(KR_0)\left(e^{-\kappa\Delta} + e^{\kappa\Delta}\right)}\right] \tag{2.117}$$

For $k \to 0$ (or $E \to 0$) we obtain $\delta_0 \to 0$.

The wave intensity in the interior region, $|A'|^2$, is found by eliminating the constants C, D, and the phase shift δ_0. Furthermore, we use the expressions $e^{2x} + e^{-2x} = 4\sinh^2 x + 2$ and $e^x - e^{-x} = 2\sinh x$. The tedious algebra is not given here explicitly. The result is

$$\begin{aligned}\frac{|F'|^2}{|A'|^2} = {} & \sin^2(KR_0) + \left(\frac{K}{k}\right)^2 \cos^2(KR_0) \\ & + \sin^2(KR_0)\sinh^2(\kappa\Delta)\left[1 + \left(\frac{\kappa}{k}\right)^2\right] \\ & + \cos^2(KR_0)\sinh^2(\kappa\Delta)\left[\left(\frac{K}{\kappa}\right)^2 + \left(\frac{K}{k}\right)^2\right] \\ & + \sin(KR_0)\cos(KR_0)\sinh(2\kappa\Delta)\left[\left(\frac{K}{\kappa}\right) + \left(\frac{K}{\kappa}\right)\left(\frac{\kappa}{k}\right)^2\right]\end{aligned} \tag{2.118}$$

The energy dependence of the quantities $|A'|^2/|F'|^2$, $|A'|^2/(|F'|^2\hat{T})$ and δ_0 for neutron scattering by a square-barrier potential is shown in Fig. 2.14, where the transmission coefficient $\hat{T}$ is obtained from the approximation of Eq. (2.109). We assume values of V_0 = 100 MeV, V_1 = 10 MeV, R_0 = 3 fm, R_1 = 8 fm (dashed lines) and V_0 = 50 MeV, V_1 = 10 MeV, R_0 = 3 fm, R_1 = 8 fm (solid lines). The figure reflects both the effects of the barrier transmission and the resonance phenomenon. For a potential depth of V_0 = 100 MeV, no resonance occurs over the energy range shown and the plot looks almost identical to the corresponding part in Fig. 2.13. Consequently, the quantity $|A'|^2/(|F'|^2\hat{T})$ is almost constant with energy. Furthermore, the phase shift varies smoothly with energy. For a potential depth of V_0 = 50 MeV, on the other hand, the

interior wave function solution has a large amplitude due to good matching conditions. The resulting resonance is clearly seen in part (a). The shape of the resonance is distorted by the barrier transmission coefficient. In part (b), the effects of the barrier transmission are removed and, consequently, the shape of the resonance becomes symmetric. It is also evident that the resonance shifts the phase by a significant amount. This method of removing the transmission coefficient from the wave function intensity or the cross section is of crucial importance in nuclear astrophysics, as will be seen in Chapter 3.

A plot of $|A'|^2/|F'|^2$ versus potential depth V_0 in the region $r < R_0$ is shown in Fig. 2.15. The graph is obtained for the potential parameters $V_1 = 10$ MeV, $R_0 = 3$ fm, $R_1 = 8$ fm, and $E = 5$ MeV. Several resonances are apparent which become broader with increasing value of V_0. By changing V_0 we change the wavelength in the interior region (see Eq. (2.81)). As was the case for the simple square-well potential (Section 2.4.1), the resonances result from favorable wave function matching conditions at the boundaries. The first resonance corresponds to a wave function with no node in the region $r < R_0$. The second resonance corresponds to one node, the third resonance to two nodes, and so on. Comparison to Fig. 2.11 shows that the resonances are much narrower because of the repulsive square-barrier potential.

As a final example, Fig. 2.16 shows schematically the radial wave functions for three cases. In part (a) the potential depth is zero. The amplitude of the wave function in the interior is very small and reflects primarily the transmission through the barrier. In part (b), the amplitude in the interior is at maximum due to favorable matching conditions. The system is in resonance with no wave function node in the interior. Part (c) displays the wave function for the second resonance, showing one node in the interior region.

2.4.3 Transmission Through the Coulomb Barrier

The low-energy s-wave transmission coefficient for a square-barrier potential (see Eq. (2.109)) can be easily generalized since a potential barrier of arbitrary shape may be divided into thin slices of width dr. The total s-wave transmission coefficient is then given by the product of the transmission coefficients for each slice,

$$\hat{T} = \hat{T}_1 \cdot \hat{T}_2 \cdot \ldots \cdot \hat{T}_n \approx \exp\left[-\frac{2}{\hbar}\sum_i \sqrt{2m(V_i - E)}(R_{i+1} - R_i)\right]$$
$$\xrightarrow[n\,\text{large}]{} \exp\left[-\frac{2}{\hbar}\int_{R_0}^{R_c} \sqrt{2m[V(r) - E]}\, dr\right] \tag{2.119}$$

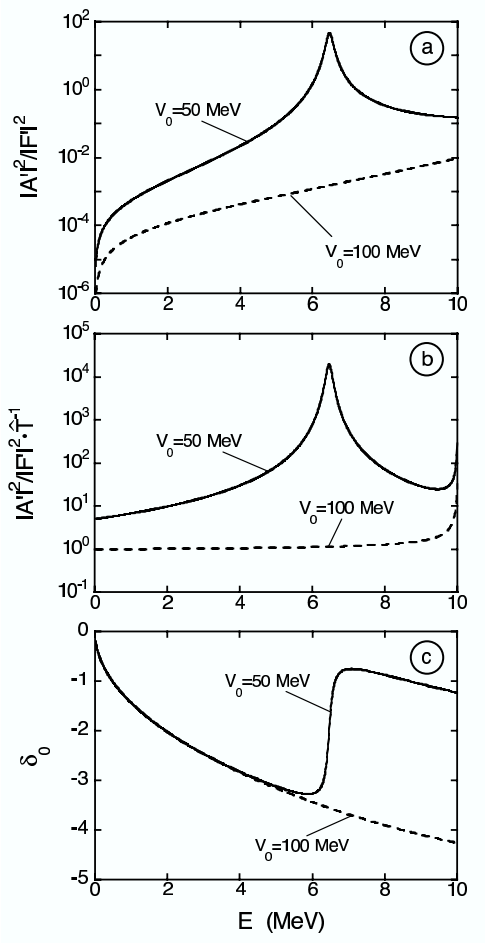

Fig. 2.14 Energy dependence of the quantities (a) $|A'|^2/|F'|^2$, (b) $|A'|^2/(|F'|^2\hat{T})$ and (c) δ_0 for neutron scattering by a square-barrier potential (Fig. 2.12). The properties of the potential are V_1 = 10 MeV, R_0 = 3 fm and R_1 = 8 fm. The dashed and solid lines are obtained for potential depths of V_0 = 100 MeV and V_0 = 50 MeV, respectively. The curves represent the effects of both the barrier transmission and the resonance phenomenon. In part (b), the effects of the barrier transmission are removed and the shape of the resonance becomes symmetric (solid line).

For the important case of the Coulomb potential, displayed in Fig. 2.17, we obtain

$$\hat{T} \approx \exp\left(-\frac{2}{\hbar}\sqrt{2m}\int_{R_0}^{R_c}\sqrt{\frac{Z_0 Z_1 e^2}{r} - E}\,dr\right) \tag{2.120}$$

with Z_0 and Z_1 the charge of the projectile and target, respectively. The quantity R_0 is the radius of the square-well potential and defines the height

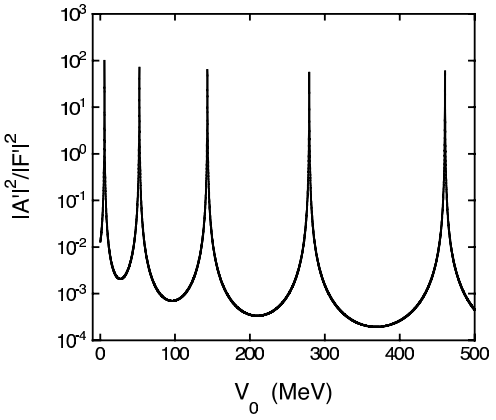

Fig. 2.15 Plot of $|A'|^2/|F'|^2$ versus potential depth V_0 in the interior region for the scattering of neutrons by a square-barrier potential. The curve is calculated for the parameters V_1 = 10 MeV, R_0 = 3 fm, R_1 = 8 fm and E = 5 MeV. The maxima correspond to resonances which result from favorable wave function matching conditions at the boundaries.

of the Coulomb barrier, $V_C = Z_0 Z_1 e^2/R_0$. Numerically, one finds $V_C = 1.44 Z_0 Z_1/R_0$ (MeV), with R_0 in units of femtometers. The quantity R_c is the distance at which the incoming particle would be reflected classically. It is referred to as *classical turning point* and is defined by $E = Z_0 Z_1 e^2/R_c$ or $E/V_C = R_0/R_c$. The integral in Eq. (2.120) can be solved analytically. Rewriting the above expression by using the definition of the classical turning point yields

$$\hat{T} \approx \exp\left(-\frac{2}{\hbar}\sqrt{2mZ_0Z_1e^2}\int_{R_0}^{R_c}\sqrt{\frac{1}{r}-\frac{1}{R_c}}\,dr\right) \tag{2.121}$$

Substitution of $z \equiv r/R_c$ gives

$$\begin{aligned}\hat{T} &\approx \exp\left(-\frac{2}{\hbar}\sqrt{2mZ_0Z_1e^2}\int_{R_0/R_c}^{1}\sqrt{\frac{1}{zR_c}-\frac{1}{R_c}}R_c\,dz\right)\\ &= \exp\left(-\frac{2}{\hbar}\sqrt{\frac{2m}{E}}Z_0Z_1e^2\int_{R_0/R_c}^{1}\sqrt{\frac{1}{z}-1}\,dz\right)\end{aligned} \tag{2.122}$$

The result is

$$\hat{T} \approx \exp\left(-\frac{2}{\hbar}\sqrt{\frac{2m}{E}}Z_0Z_1e^2\left[\arccos\sqrt{\frac{E}{V_C}}-\sqrt{\frac{E}{V_C}\left(1-\frac{E}{V_C}\right)}\right]\right) \tag{2.123}$$

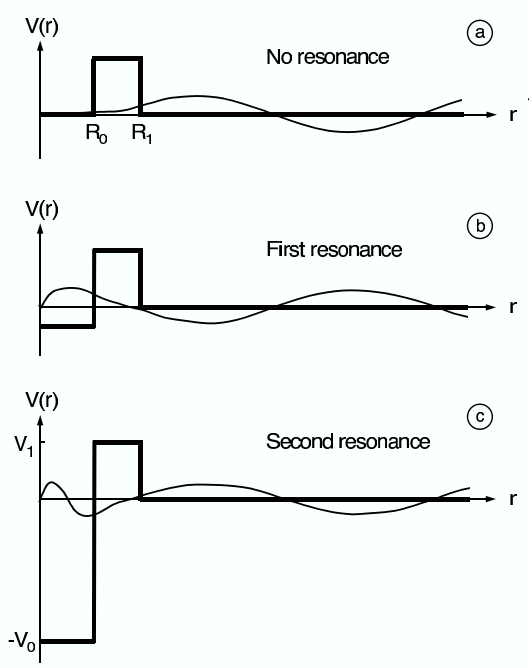

Fig. 2.16 Schematic representation of radial wave functions (thin solid lines) for the scattering of neutral particles by a square-barrier potential (thick solid line) of different potential depths V_0. The wave functions are appropriate for (a) no resonance, (b) the first resonance with no wave function node in the interior region ($r < R_0$), and (c) the second resonance with one node in the interior.

For low energies compared to the Coulomb barrier height, $E/V_C \ll 1$, we use the expansion $\arccos\sqrt{x} - \sqrt{x(1-x)} \approx \pi/2 - 2\sqrt{x} + x^{3/2}/3$ and obtain

$$\hat{T} \approx \exp\left(-\frac{2}{\hbar}\sqrt{\frac{2m}{E}}Z_0Z_1e^2\left[\frac{\pi}{2} - 2\sqrt{\frac{E}{V_C}} + \frac{1}{3}\left(\frac{E}{V_C}\right)^{3/2}\right]\right)$$
$$= \exp\left(-\frac{2\pi}{\hbar}\sqrt{\frac{m}{2E}}Z_0Z_1e^2\left[1 + \frac{2}{3\pi}\left(\frac{E}{V_C}\right)^{3/2}\right] + \frac{4}{\hbar}\sqrt{2mZ_0Z_1e^2R_0}\right) \quad (2.124)$$

The first term in the exponential is larger than the third term by a factor of $(\pi/4)\sqrt{V_C/E}$ and therefore dominates the transmission coefficient. The third term vanishes in the limit $R_0 \to 0$ and represents a correction due to a finite radius to which the projectile must penetrate. The larger the radius R_0, the smaller the penetration distance (Fig. 2.17) and the larger the transmission coefficient will become. The second term represents a correction factor to the first term when the energy becomes a significant fraction of the Coulomb

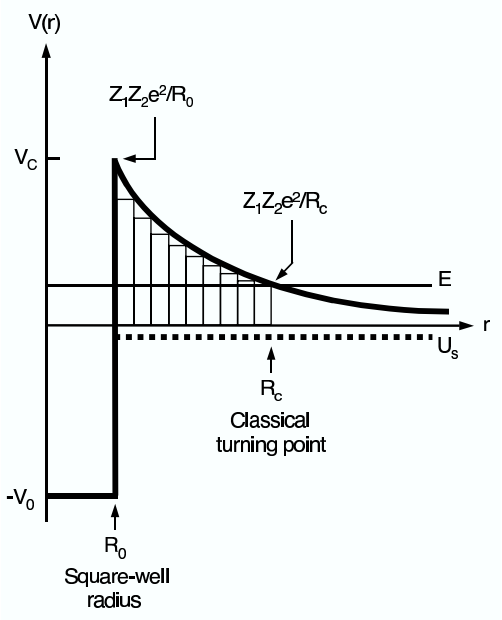

Fig. 2.17 Attractive nuclear square-well potential ($r < R_0$) plus repulsive Coulomb potential ($r > R_0$), shown as thick solid line. The transmission coefficient can be calculated analytically by dividing the Coulomb barrier of height $V_C = Z_1 Z_2 e^2 / R_0$ into infinitesimally thin square-barrier potentials. The radius R_c at which the total particle energy E (thin solid line) is equal to the Coulomb potential, $E = Z_1 Z_2 e^2 / R_c$, is referred to as the classical turning point. The thick dashed line indicates a small negative (attractive) potential U_s that results from the polarization of the electron–ion plasma (electron screening), giving rise to a modification of both the Coulomb potential and the energetics of the reaction (Section 3.2.6).

barrier height. The leading term of the s-wave Coulomb barrier transmission coefficient for small energies compared to the Coulomb barrier height,

$$\hat{T} \approx \exp\left(-\frac{2\pi}{\hbar}\sqrt{\frac{m}{2E}} Z_0 Z_1 e^2\right) \equiv e^{-2\pi\eta} \tag{2.125}$$

is called the *Gamow factor* and will play an important role in the discussion of thermonuclear reaction rates for charged particles (Section 3.2.1). The quantity η is the Sommerfeld parameter. Numerically, we find

$$2\pi\eta = 0.989534 Z_0 Z_1 \sqrt{\frac{1}{E}\frac{M_0 M_1}{M_0 + M_1}} \tag{2.126}$$

where the energy E is in MeV and the relative atomic masses M_i are in units of u.

2.5 Theory of Resonances

2.5.1 General Aspects

Up to now we have discussed wave function intensities, phase shifts, and transmission probabilities for simple nuclear potentials. In the following, the resulting cross sections will be considered. Initially, we will restrict ourselves again to the case of s-wave scattering of neutral particles, that is, the complications of the Coulomb and centripetal barriers are disregarded. The total elastic scattering and reaction cross sections are then given by Eqs. (2.40) and (2.49),

$$\sigma_{\mathrm{el},0} = \frac{\pi}{k^2}\left|1 - e^{2i\delta_0}\right|^2 = \frac{4\pi}{k^2}\sin^2\delta_0 \tag{2.127}$$

$$\sigma_{\mathrm{re},0} = \frac{\pi}{k^2}\left(1 - \left|e^{2i\delta_0}\right|^2\right) \tag{2.128}$$

The cross sections are entirely determined by the phase shift δ_0.

It is interesting to plot the total elastic scattering cross sections for the potential models considered in Sections 2.4.1 and 2.4.2. They are shown in Fig. 2.18 for (a) a square-well potential with R_0 = 3 fm, V_0 = 100 MeV; (b) a square-barrier potential with R_0 = 3 fm, R_1 = 8 fm, V_0 = 100 MeV, V_1 = 10 MeV; and (c) a square-barrier potential with R_0 = 3 fm, R_1 = 8 fm, V_0 = 50 MeV, V_1 = 10 MeV. We expect resonances in parts (a) and (c), as is apparent from Figs. 2.8 and 2.14. However, a resonance is clearly observed only in Fig. 2.18c. And even in this case the resulting shape of the total elastic scattering cross section looks complicated.

Up to now we considered single-particle potentials. The spacing of resonances, referred to as single-particle resonances, calculated by these models amounts to many MeV. However, experiments performed since the 1930s frequently showed closely spaced resonances (sometimes a few keV or less apart) of very narrow widths. For example, Fig. 2.19 shows the experimental elastic scattering cross section of neutrons on ^{16}O. In contrast to our theoretical results obtained so far, a very complicated structure consisting of several resonances with different widths is clearly observed. The solid line in Fig. 2.19 represents a calculation using a single-particle potential. It reproduces only one of the many resonances shown. Although some observed resonances can indeed be described by single-particle potentials, in the vast majority of cases the single-particle picture is clearly not appropriate for the explanation of the observed rapid cross section variations.

At this point we suspect that the interactions of many nucleons inside the nucleus are complicated and cannot be expressed in terms of a single radial wave function generated by a single-particle potential. In the following, we

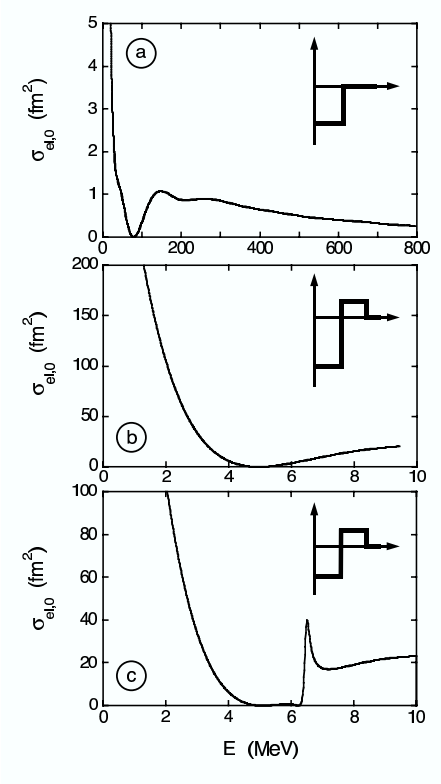

Fig. 2.18 Elastic scattering cross sections for s-wave neutrons versus energy for the simple potentials discussed in Sections 2.4.1 and 2.4.2: (a) square-well potential with R_0 = 3 fm, V_0 = 100 MeV; (b) square-barrier potential with R_0 = 3 fm, R_1 = 8 fm, V_0 = 100 MeV, V_1 = 10 MeV; (c) square-barrier potential with R_0 = 3 fm, R_1 = 8 fm, V_0 = 50 MeV, V_1 = 10 MeV. A resonance is clearly observed only in part (c).

will develop a different model in order to describe a nuclear resonance in general terms without using an explicit assumption for the nuclear potential. In fact, a specific assumption regarding the many-particle nuclear potential may even be undesirable since at this point neither the nuclear forces between the nucleons nor their motion in the nuclear interior are precisely known.

2.5.2
Logarithmic Derivative, Phase Shift, and Cross Section

Since we will not make reference to a specific nuclear potential, this model will not be able to predict the absolute magnitude of cross sections. In fact, most

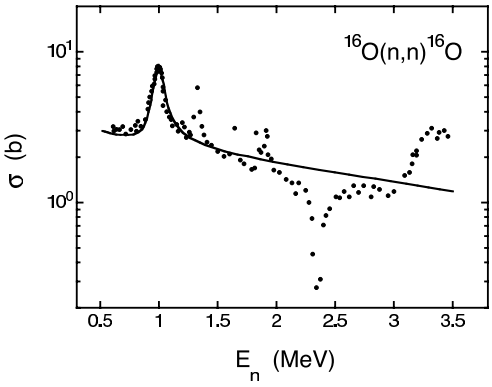

Fig. 2.19 Experimental total cross section for the elastic scattering ^{16}O(n,n)^{16}O (data points) and calculated elastic scattering cross section using a (Woods–Saxon) single-particle potential (solid line). The potential reproduces only one of the observed resonances but cannot account for the entire observed structure. Reprinted with permission from G. D. Westin and J. L. Adams, Phys. Rev. C, Vol. 4, p. 363 (1972). Copyright (1972) by the American Physical Society.

resonance theories reformulate the cross sections in terms of known quantities of the nuclear exterior (penetration and shift factors) and unknown quantities of the nuclear interior (reduced widths). Our goal is to predict relative cross sections "near" a resonance. The only assumptions we make regarding the nuclear potential is the existence of a relatively well-defined spherical nuclear surface at $r = R$ and that the projectile and target have no nuclear interaction outside of this radius.

At this boundary the interior and exterior wave functions and their derivatives have to be matched,

$$u_\ell^{\text{in}}(R) = u_\ell^{\text{out}}(R) \qquad \text{and} \qquad \left(\frac{du_\ell^{\text{in}}(r)}{dr}\right)_{r=R} = \left(\frac{du_\ell^{\text{out}}(r)}{dr}\right)_{r=R} \tag{2.129}$$

By dividing both expressions and by introducing a dimensionless quantity, called the *logarithmic derivative at the boundary*,

$$f_\ell \equiv R\left(\frac{1}{u_\ell(r)}\frac{du_\ell(r)}{dr}\right)_{r=R} = R\left(\frac{d\ln u_\ell(r)}{dr}\right)_{r=R} \tag{2.130}$$

we can rewrite the conditions of Eq. (2.129) as

$$f_\ell(u_\ell^{\text{in}}) = f_\ell(u_\ell^{\text{out}}) \tag{2.131}$$

In other words, the calculation of f_ℓ with u_ℓ^{in} and u_ℓ^{out} must yield the same value. Obviously, the quantity f is related to the slope of the wave function at the radius $r = R$.

We start from the expression for the total wave function in the exterior region $r > R$ (see Eq. (2.32)). For s-waves ($\ell = 0$) it reduces to

$$\begin{aligned}\psi_{T,\text{out}} &= Ae^{ikr} + Be^{-ikr}, \qquad k^2 = \frac{2mE}{\hbar^2} \\ &= -\frac{i}{2kr}\, e^{2i\delta_0} e^{ikr} + \frac{i}{2kr}\, e^{-ikr} = \frac{i}{2kr}\left(e^{-ikr} - e^{2i\delta_0} e^{ikr}\right) \\ &= \frac{1}{2kr}\, e^{i\delta_0}\left[e^{-i(kr+\delta_0)} - e^{i(kr+\delta_0)}\right] = \frac{1}{kr}\, e^{i\delta_0} \sin(kr + \delta_0) \end{aligned} \tag{2.132}$$

where the first expression ($Ae^{ikr} + Be^{-ikr}$) generally holds in the force-free region (Eqs. (2.57) and (2.86); see also Appendix A.1). Recall the meaning of the above equation. The outgoing spherical wave e^{ikr} is multiplied by a factor $e^{2i\delta_0}$ which effectively shifts the wave by an amount of δ_0.

As already implied in Sections 2.3.3 and 2.3.4, for the special case of s-waves, Eq. (2.32) (and thus Eq. (2.132)) is not only valid at large distances but applies to all distances $r > R$. Furthermore, the spherical harmonic for $\ell = 0$ is constant (see Eq. (A.9)) and, therefore, the total wave function is given by the radial wave function

$$\psi_{T,\text{out}} = \frac{i}{2kr}\left(e^{-ikr} - e^{2i\delta_0} e^{ikr}\right) = \frac{u_{\text{out}}(r)}{r} \tag{2.133}$$

The cross section is determined by the phase shift δ_0. We will first find a relationship between δ_0 and f_0 and will then express the cross section in terms of f_0. From Eqs. (2.130) and (2.133) one obtains

$$\frac{f_0}{R} = \left(\frac{1}{u_{\text{out}}(r)} \frac{du_{\text{out}}(r)}{dr}\right)_{r=R} = \frac{-ike^{-ikR} - ike^{2i\delta_0} e^{ikR}}{e^{-ikR} - e^{2i\delta_0} e^{ikR}} \tag{2.134}$$

Solving for $e^{2i\delta_0}$ gives

$$e^{2i\delta_0} = \frac{f_0 + ikR}{f_0 - ikR}\, e^{-2ikR} \tag{2.135}$$

For the elastic scattering cross section (see Eq. (2.127)) we find

$$\begin{aligned}\sigma_{\text{el},0} &= \frac{\pi}{k^2}\left|1 - \frac{f_0 + ikR}{f_0 - ikR} e^{-2ikR}\right|^2 = \frac{\pi}{k^2}\left|e^{2ikR} - \frac{f_0 + ikR}{f_0 - ikR}\right|^2 \\ &= \frac{\pi}{k^2}\left|-\frac{2ikR}{f_0 - ikR} + e^{2ikR} - 1\right|^2 = \frac{\pi}{k^2}\left|A_{\text{res}} + A_{\text{pot}}\right|^2 \end{aligned} \tag{2.136}$$

with

$$A_{\text{res}} = -\frac{2ikR}{f_0 - ikR} \qquad \text{and} \qquad A_{\text{pot}} = e^{2ikR} - 1 \tag{2.137}$$

It can be seen that A_{res} has a maximum if $f_0 = 0$, consistent with our identification of resonances as a slope of zero for the radial wave function at the boundary $r = R$.

Similarly, using $f_0 = \text{Re}\, f_0 + i\, \text{Im}\, f_0 = g + ih$, one obtains for the reaction cross section (see Eq. (2.128))

$$\begin{aligned}\sigma_{\text{re},0} &= \frac{\pi}{k^2}\left(1 - \left|\frac{f_0 + ikR}{f_0 - ikR}e^{-2ikR}\right|^2\right) \\ &= \frac{\pi}{k^2}\left[1 - \left(\frac{g + ih + ikR}{g + ih - ikR}\right)\left(\frac{g - ih - ikR}{g - ih + ikR}\right)\right] \\ &= \frac{\pi}{k^2}\frac{-4hkR}{g^2 + h^2 - 2hkR + k^2R^2} = \frac{\pi}{k^2}\frac{-4kR\,\text{Im}\, f_0}{(\text{Re}\, f_0)^2 + (\text{Im}\, f_0 - kR)^2}\end{aligned} \tag{2.138}$$

Only A_{res} depends on the interior region $r < R$ through f_0. Consequently, only this term can give rise to resonances and A_{res} is called *resonance scattering amplitude*. The term A_{pot} can be interpreted as follows. Suppose that $f_0 \to \infty$. In that case $A_{\text{res}} = 0$. From the definition of f_0 (see Eq. (2.130)) this implies $u(R) = 0$ and, therefore, an infinitely high potential for $r < R$ (that is, the sphere of radius R is impenetrable). Thus, the quantity A_{pot} is called *hard-sphere potential scattering amplitude*. Note also that $\text{Im}\, f_0 \leq 0$; otherwise $\sigma_{\text{re},0}$ becomes negative. For the special case that f_0 is real ($\text{Im}\, f_0 = 0$), the reaction cross section disappears, $\sigma_{\text{re},0} = 0$. Therefore, f_0 must be complex for reactions to occur.

It is also interesting to consider the elastic scattering phase shift δ_0. From Eq. (2.135) one finds

$$2i\delta_0 = \ln(f_0 + ikR) - \ln(f_0 - ikR) - 2ikR \tag{2.139}$$

Assuming $\text{Im}\, f_0 = 0$ (or $\sigma_{\text{re},0} = 0$) we find by using the identity $\ln(a + ib) = (1/2)\ln(a^2 + b^2) + i\arctan(b/a)$

$$\begin{aligned}\delta_0 &= \frac{1}{2i}\left[\frac{1}{2}\ln\left(f_0^2 + k^2R^2\right) + i\arctan\left(\frac{kR}{f_0}\right)\right] \\ &\quad - \frac{1}{2i}\left[\frac{1}{2}\ln\left(f_0^2 + k^2R^2\right) + i\arctan\left(\frac{-kR}{f_0}\right)\right] - kR \\ &= \arctan\left(\frac{kR}{f_0}\right) - kR = \beta_0 + \varphi_0\end{aligned} \tag{2.140}$$

with

$$\beta_0 = \arctan\left(\frac{kR}{f_0}\right) \qquad \text{and} \qquad \varphi_0 = -kR \tag{2.141}$$

The phase shift δ_0 is expressed as a sum of two terms. The first term, β_0, depends on the scattering potential through f_0 and can give rise to resonances.

The second term, φ_0, is independent of the scattering potential. It corresponds to the phase shift for hardsphere scattering, since $\delta_0 = \varphi_0$ for $f_0 \to \infty$ (or $u(R) = 0$).

2.5.3 Breit–Wigner Formulas

The logarithmic derivative at the boundary, f_0, has to be known in order to calculate $\sigma_{\mathrm{el},0}$ and $\sigma_{\mathrm{re},0}$. For the derivation of f_0 we need to make some assumptions regarding the wave function in the nuclear interior ($r < R$). Remember that the general solution with constant wave number K in the interior (see Eqs. (2.55) and (2.84))

$$u_{\mathrm{in}} = Ae^{iKr} + Be^{-iKr} \tag{2.142}$$

only applies for the simple assumption of a constant potential $V(r) = \mathrm{const}$ (Section 2.4). Clearly, the actual nuclear potential will be rather complicated since for $r < R$ the wave function of the incident particle will depend on the variables of all the other nucleons involved. Nevertheless, we will approximate the interior wave function, in the closest vicinity of the nuclear boundary only, by the above expression.

The complex amplitudes A and B depend on the properties of the nuclear system. We have to allow for a phase difference ζ between incoming (e^{-iKr}) and outgoing (e^{iKr}) spherical waves. Furthermore, one has to account for the possibility that the particle is absorbed in the nuclear interior due to reaction processes, that is, the amplitude of the outgoing wave e^{iKr} will generally be smaller than the amplitude of the incoming wave e^{-iKr}. We start with the ansatz

$$A = Be^{2i\zeta}e^{-2q} \tag{2.143}$$

where both ζ and q are real numbers. We also require $q \geq 0$ since no more particles can return than entered the nucleus originally. From Eqs. (2.142) and (2.143) one finds

$$\begin{aligned} u_{\mathrm{in}} &= Be^{2i\zeta}e^{-2q}e^{iKr} + Be^{-iKr} = \frac{B}{2}\left[e^{-i(Kr+\zeta+iq)} + e^{i(Kr+\zeta+iq)}\right] 2e^{(i\zeta-q)} \\ &= 2Be^{(i\zeta-q)}\cos(Kr+\zeta+iq) \end{aligned} \tag{2.144}$$

The logarithmic derivative of the radial wave function must be continuous at $r = R$. Substitution of Eq. (2.144) into Eq. (2.130) yields

$$\begin{aligned} f_0 &= R\left(\frac{1}{u_{\mathrm{in}}(r)}\frac{du_{\mathrm{in}}(r)}{dr}\right)_{r=R} = R\frac{-2Be^{(i\zeta-q)}K\sin(KR+\zeta+iq)}{2Be^{(i\zeta-q)}\cos(KR+\zeta+iq)} \\ &= -KR\tan(KR+\zeta+iq) \end{aligned} \tag{2.145}$$

Clearly, f_0 depends on the energy-dependent quantities K, ζ, and q. If one knew these variables, then one could calculate resonance energies and cross sections directly from the properties of the nuclear interior. Unfortunately, this is not the case. Thus, our strategy will be to express the cross sections σ_{el} and σ_{re} near a single resonance in terms of measurable quantities.

We will assume that the argument of the tangent, $KR + \zeta + iq$, is a smooth function of energy E. Furthermore, if $q = 0$ then f_0 becomes real, and the reaction cross section disappears. Recall that a resonance corresponds to a large wave function amplitude in the nuclear interior, implying a slope of zero for the radial wave function at $r = R$ (Fig. 2.10). One can define *formal resonance energies* E_λ by the condition

$$f_0(E_\lambda, q) = -KR \tan(KR + \zeta + iq) = 0 \tag{2.146}$$

Of course, there is a whole set of such energies. Let us consider any one of them and study the behavior of f_0 near E_λ.

In the following it is assumed that the absorption in the nuclear interior is weak compared to the elastic scattering process, that is $|q| \ll 1$. Expansion of $f_0(E, q)$ near E_λ and $q = 0$ into a Taylor series in both q and E gives

$$f_0 \approx f_0(E_\lambda, q) + (E - E_\lambda) \left(\frac{\partial f_0}{\partial E}\right)_{E_\lambda, q=0} + q \left(\frac{\partial f_0}{\partial q}\right)_{E_\lambda, q=0} \tag{2.147}$$

For the last term, one finds with Eq. (2.145)

$$q \left(\frac{\partial f_0}{\partial q}\right)_{E_\lambda, q=0} = -qKR \left[\frac{\partial}{\partial q} \tan(KR + \zeta + iq)\right]_{E_\lambda, q=0} = -iqKR \tag{2.148}$$

since at the resonance energy E_λ one has $\tan x = 0$ (see Eq. (2.146)) and thus $d(\tan x)/dx = \cos^{-2} x = 1$. It follows

$$f_0 \approx (E - E_\lambda) \left(\frac{\partial f_0}{\partial E}\right)_{E_\lambda, q=0} - iqKR = \mathrm{Re}\, f_0 + i\, \mathrm{Im}\, f_0 \tag{2.149}$$

Recall that $(\partial f_0/\partial E)_{E_\lambda, q=0}$ is a real quantity since $q = 0$ implies a vanishing reaction cross section. Substitution of Eq. (2.149) into Eqs. (2.137) and (2.138) gives for the resonance scattering amplitude and the reaction cross section

$$A_{\mathrm{res}} = \frac{-\frac{2ikR}{(\partial f_0/\partial E)_{E_\lambda, q=0}}}{(E - E_\lambda) - \frac{i(kR + qKR)}{(\partial f_0/\partial E)_{E_\lambda, q=0}}} \tag{2.150}$$

$$\sigma_{\mathrm{re},0} = \frac{\pi}{k^2} \frac{\frac{(2kR)(2qKR)}{(\partial f_0/\partial E)^2_{E_\lambda, q=0}}}{(E - E_\lambda)^2 + \frac{(qKR + kR)^2}{(\partial f_0/\partial E)^2_{E_\lambda, q=0}}} \tag{2.151}$$

We introduce the following definitions (the subscripts e and r stand for "elastic" and "reaction," respectively):

$$\Gamma_{\lambda e} \equiv -\frac{2kR}{(\partial f_0/\partial E)_{E_\lambda, q=0}} \qquad \text{(particle width)} \tag{2.152}$$

$$\Gamma_{\lambda r} \equiv -\frac{2qKR}{(\partial f_0/\partial E)_{E_\lambda, q=0}} \qquad \text{(reaction width)} \tag{2.153}$$

$$\Gamma_\lambda \equiv \Gamma_{\lambda e} + \Gamma_{\lambda r} \qquad \text{(total width)} \tag{2.154}$$

Only the quantity $\Gamma_{\lambda r}$ depends on the parameter q describing absorption in the nuclear interior. The new quantities $\Gamma_{\lambda e}$, $\Gamma_{\lambda r}$, and Γ_λ have units of energy since f_0, kR, and KR are dimensionless. All widths refer to the resonance λ of interest. Also, f_0 depends on the channel through which the reaction is initiated. Rewriting Eqs. (2.150) and (2.151) in terms of the newly defined quantities yields, after some algebra, for the elastic scattering and reaction cross sections (see Eqs. (2.136) and (2.138))

$$\begin{aligned}\sigma_{el,0} &= \frac{\pi}{k^2}\left|\frac{i\Gamma_{\lambda e}}{(E-E_\lambda)+i\Gamma_\lambda/2} + e^{2ikR} - 1\right|^2 \\ &= \frac{\pi}{k^2}\Bigg[2 - 2\cos(2kR) \\ &\quad + \frac{\Gamma_{\lambda e}^2 - \Gamma_{\lambda e}\Gamma_\lambda + \Gamma_{\lambda e}\Gamma_\lambda\cos(2kR) + 2\Gamma_{\lambda e}(E-E_\lambda)\sin(2kR)}{(E-E_\lambda)^2 + \Gamma_\lambda^2/4}\Bigg]\end{aligned} \tag{2.155}$$

$$\sigma_{re,0} = \frac{\pi}{k^2}\frac{\Gamma_{\lambda e}\Gamma_{\lambda r}}{(E-E_\lambda)^2 + \Gamma_\lambda^2/4} \tag{2.156}$$

The last two expressions are referred to as *Breit–Wigner formulas* for s-wave neutrons.

Plots of $\sigma_{el,0}$ and $\sigma_{re,0}$ for incident neutrons versus energy E near a resonance are shown in Fig. 2.20. We use the values R = 3 fm and E_λ = 1 MeV and assume energy-independent partial widths of Γ_λ = 10.1 keV and $\Gamma_{\lambda e}$ = 10 keV. Several interesting aspects can be noticed. First, the full width at half maximum of the $\sigma_{re,0}$ curve (FWHM = 10.1 keV) corresponds precisely to the value of Γ_λ. Therefore, we identify this parameter with the *total resonance width*. The quantities $\Gamma_{\lambda e}$ and $\Gamma_{\lambda r}$ correspond then to *partial widths* for the scattering and reaction channel, respectively. Second, far away from the resonance ($|E - E_\lambda| \gg \Gamma_\lambda$) only the hardsphere potential scattering amplitude A_{pot} will contribute to the cross section. We obtain from Eq. (2.155) a value of $\sigma_{el,0} \approx (2\pi/k^2)[1 - \cos(2kR)] \approx 100$ fm^2, shown as dashed line in Fig. 2.20. Third, the numerator in the expression for $\sigma_{el,0}$ (see Eq. (2.155)) contains an interference term $2\Gamma_{\lambda e}(E - E_\lambda)\sin(2kR)$ which will change sign below and above the resonance. Clearly, the structure seen in Fig. 2.20a is caused by destructive

($E < E_\lambda$) and constructive ($E > E_\lambda$) interference of A_{res} and A_{pot}. This interference also causes the full width at half maximum in the elastic scattering cross section at the resonance to be different from the value of Γ_λ. Fourth, remember that a resonance corresponds to a value of zero for the logarithmic derivative f_0 at the nuclear boundary. The implication is that in the scattering process the particle enters the nucleus with significant probability only near resonance. Off resonance the particle is almost entirely reflected at the boundary, and the wave function inside is weak. The resonance scattering is thus ascribed to the inside of the nucleus and the potential scattering to its surface.

The present results help us understand the complicated structures observed in the scattering cross sections for an explicit nuclear potential, as shown in Fig. 2.18. The structures are caused, in part, by interference effects between the re-emission of the incident particle by the nucleus and the scattering near the nuclear surface. An additional complication is introduced by the fact that single-particle potential models predict several resonances that may interfere with each other.

We consider now the elastic scattering phase shift near a resonance, $\delta_0 = \beta_0 + \varphi_0 \approx \beta_0$. For $\operatorname{Im} f_0 = 0$ ($q = 0$) we obtain from Eqs. (2.140), (2.149), and (2.152)

$$\beta_0 \approx \arctan\left[\frac{kR}{(E - E_\lambda)(\partial f_0/\partial E)_{E_\lambda, q=0}}\right] = \arctan\left[\frac{\Gamma_{\lambda e}}{2(E_\lambda - E)}\right] \tag{2.157}$$

At the resonance energy, $E = E_\lambda$, the argument of the arctan function becomes infinite and thus $\beta_0 = \pi/2$. Furthermore, since $d(\arctan x)/dx = (1 + x^2)^{-1}$, one finds for the energy derivative of the resonance elastic scattering phase shift at $E = E_\lambda$

$$\left(\frac{d\beta_0}{dE}\right)_{E_\lambda} = \frac{1}{2}\left[\frac{(d\Gamma_{\lambda e}/dE)(E_\lambda - E) + \Gamma_{\lambda e}}{(E_\lambda - E)^2 + (\Gamma_{\lambda e}/2)^2}\right]_{E_\lambda} = \frac{2}{(\Gamma_{\lambda e})_{E_\lambda}} \tag{2.158}$$

Hence, the resonance phase shift at $E = E_\lambda$ amounts to $\pi/2$ while its energy derivative determines the particle width. For the special case that $\Gamma_{\lambda e}$ is nearly constant with energy (for example, for a narrow resonance), we find from Eq. (2.157) that $\beta_0 = \pi/4$ at $E = E_\lambda - \Gamma_{\lambda e}/2$ and $\beta_0 = 3\pi/4$ at $E = E_\lambda + \Gamma_{\lambda e}/2$. Thus the particle width $\Gamma_{\lambda e}$ becomes equal to the energy interval over which β_0 increases from $\pi/4$ to $3\pi/4$. The above techniques involving the resonance phase shift are frequently employed for the calculation of particle partial widths.

Let us now consider the particle width $\Gamma_{\lambda e}$ in more detail. We define (see Eq. (2.152))

$$\Gamma_{\lambda e} = -\frac{2kR}{(\partial f_0/\partial E)_{E_\lambda, q=0}} \equiv 2P_0\gamma_{\lambda e}^2 \quad \text{with} \quad \gamma_{\lambda e}^2 \equiv -\left(\frac{\partial f_0}{\partial E}\right)^{-1}_{E_\lambda, q=0} \tag{2.159}$$

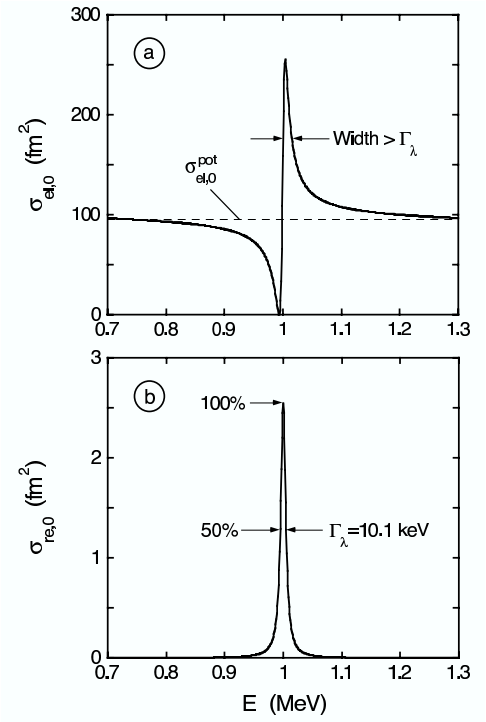

Fig. 2.20 Plots of (a) $\sigma_{\mathrm{el},0}$ and (b) $\sigma_{\mathrm{re},0}$ versus energy E for incident neutrons near a resonance at E_λ = 1 MeV. A value of R = 3 fm is chosen for the radius. The widths are assumed to be energy independent with values of Γ_λ = 10.1 keV and $\Gamma_{\lambda\mathrm{e}}$ = 10 keV. See discussion in the text.

where the particle width has been split into two factors. The first factor, $P_0 = kR$, depends on the channel energy through the factor kR and on the conditions outside the nucleus. The second factor, $\gamma^2_{\lambda\mathrm{e}}$, is called the *reduced width* and it incorporates all the unknown properties of the nuclear interior. The quantity $\gamma^2_{\lambda\mathrm{e}}$ is characteristic of the resonance and the channel under consideration, and is independent of the channel energy E. The energy dependence of the partial widths $\Gamma_{\lambda\mathrm{e}}$ and $\Gamma_{\lambda\mathrm{r}}$ has to be taken into account when calculating the cross section for broad resonances, as will be explained in later sections.

2.5.4
Extension to Charged Particles and Arbitrary Values of Orbital Angular Momentum

The one-level Breit–Wigner formulas (see Eqs. (2.155) and (2.156)) have been obtained near a formal resonance energy E_λ assuming (i) neutrons as incident

particles, (ii) an orbital angular momentum of $\ell = 0$, and (iii) interactions of spinless particles. The basic structure of the cross section expressions derived here is also applicable to the much more general case. Although the general expressions are more complicated in appearance compared to the results for s-wave neutrons, no new physical ideas are involved. The properties of the nuclear interior enter into the cross sections only through the logarithmic derivative f_ℓ of the wave function $u_\ell(r)$ at the nuclear boundary $r = R$.

In the following, the formulas will be generalized to arbitrary values of ℓ and to interacting charged particles. We will not derive the results in detail here (see, for example, Blatt and Weisskopf 1952) but will only sketch some results of the derivation. Of special interest to us is the modified reaction cross section $\sigma_{\mathrm{re},\ell}$.

The radial wave function solutions of the Schrödinger equation outside the nuclear surface are no longer given by incoming and outgoing spherical waves (e^{-ikr} and e^{ikr}), as in the case of $\ell = 0$ neutrons (see Eq. (2.132)), but are given in terms of the functions F_ℓ and G_ℓ. For neutrons, these represent spherical Bessel and Neumann functions, $F_\ell = (kr)j_\ell(kr)$ and $G_\ell = (kr)n_\ell(kr)$, respectively, while for charged particles they correspond to the regular and irregular Coulomb wave functions (Appendix A.3). The radial wave function outside the nuclear boundary is given in terms of F_ℓ and G_ℓ by

$$\begin{aligned} u_\ell(r) &= Au_\ell^+(r) + Bu_\ell^-(r), \qquad r > R \\ &= Ae^{-i\sigma_\ell}[G_\ell(r) + iF_\ell(r)] + Be^{i\sigma_\ell}[G_\ell(r) - iF_\ell(r)] \end{aligned} \tag{2.160}$$

where u_ℓ^- and u_ℓ^+ correspond, for large distances, to incoming and outgoing spherical waves, respectively. The quantity σ_ℓ denotes the Coulomb phase shift and determines the purely Rutherford (electrostatic) scattering. For $\ell = 0$ neutrons, the above expression reduces to our previous result (Eq. (2.132); see Problem 2.4).

It is of advantage to introduce two real quantities, called *shift factor* S_ℓ and *penetration factor* P_ℓ, which are completely determined by the conditions outside the nucleus. We obtain with Eqs. (2.160) and (A.18)

$$\begin{aligned} &R\left(\frac{1}{u_\ell^+(r)}\frac{du_\ell^+(r)}{dr}\right)_{r=R} \\ &\quad = R\left[\frac{G_\ell(dG_\ell/dr) + F_\ell(dF_\ell/dr) + iG_\ell(dF_\ell/dr) - iF_\ell(dG_\ell/dr)}{F_\ell^2 + G_\ell^2}\right]_{r=R} \\ &\quad \equiv S_\ell + iP_\ell \end{aligned} \tag{2.161}$$

where

$$S_\ell = R\left[\frac{F_\ell(dF_\ell/dr)+G_\ell(dG_\ell/dr)}{F_\ell^2+G_\ell^2}\right]_{r=R} \quad \text{and}$$
$$P_\ell = R\left(\frac{k}{F_\ell^2+G_\ell^2}\right)_{r=R} \tag{2.162}$$

The new quantities depend on the wave number k, the channel radius R, the orbital angular momentum ℓ, and on the charge parameter η (see Eq. (A.32)). For $\ell = 0$ neutrons, $F_\ell = (kr)j_0(kr) = \sin(kr)$ and $G_\ell = (kr)n_0(kr) = \cos(kr)$ (Appendix A.2), and we obtain from Eq. (2.161) $P_0 = kR$ and $S_0 = 0$. In other words, the shift factor vanishes if there is no barrier. With the quantities P_ℓ and S_ℓ, the reaction cross section can be derived in a similar way as presented in the previous section. The calculation is not repeated here (see Blatt and Weisskopf 1952). The result is the Breit–Wigner formula

$$\sigma_{\mathrm{re},\ell} = (2\ell+1)\frac{\pi}{k^2}\frac{\Gamma_{\lambda\mathrm{e}}\Gamma_{\lambda\mathrm{r}}}{(E-E_r)^2+\Gamma_\lambda^2/4} \tag{2.163}$$

with

$$\Gamma_{\lambda\mathrm{e}} \equiv -\frac{2P_\ell(E)}{(\partial f_\ell/\partial E)_{E_\lambda,q=0}} = 2P_\ell(E)\gamma_{\lambda\mathrm{e}}^2 \qquad \text{(particle width)} \tag{2.164}$$

$$\Gamma_{\lambda\mathrm{r}} \equiv -\frac{2qKR}{(\partial f_\ell/\partial E)_{E_\lambda,q=0}} \qquad \text{(reaction width)} \tag{2.165}$$

$$\Gamma_\lambda = \Gamma_{\lambda\mathrm{e}} + \Gamma_{\lambda\mathrm{r}} \qquad \text{(total width)} \tag{2.166}$$

$$E_r \equiv E_\lambda + \frac{S_\ell(E)}{(\partial f_\ell/\partial E)_{E_\lambda,q=0}} = E_\lambda - S_\ell(E)\gamma_{\lambda\mathrm{e}}^2 \qquad \text{(observed resonance energy)} \tag{2.167}$$

The similarity between Eq. (2.163) and the result obtained earlier for s-wave neutrons (see Eq. (2.156)) is apparent. The meaning of P_ℓ and S_ℓ becomes clear now. The penetration factor appears in the particle width expression since an incident particle must penetrate to the nuclear surface for a reaction to occur. The shift factor appears in the level shift expression and it causes the observed resonance energy E_r to be different from the formal resonance energy (or level energy) E_λ. Both the resonance energy shift and the particle width also depend on the properties of the nuclear interior through the reduced width $\gamma_{\lambda\mathrm{e}}^2$.

The penetration factor is closely related to the transmission coefficient. Both quantities describe the same physical concept, but are defined in slightly different ways. The former quantity is independent of the nuclear interior while the latter is defined in terms of the ratio of current densities in the interior and exterior regions (see Eqs. (2.62) and (2.103)). However, the energy dependences of both quantities should be very similar. The penetration factor can

be calculated analytically for neutrons. The expressions are not repeated here (see Blatt and Weisskopf 1952). It is sufficient to mention that for small neutron energies the neutron partial widths behave as $\Gamma_\ell(E) \sim P_\ell(E) \sim (kR)^{2\ell+1} \sim E^{\ell+1/2}$. For charged particles, on the other hand, the calculation of penetration factors is much more involved. Various analytical approximations exist for estimating $P_\ell(E)$ (see, for example, Clayton 1983). The reader should be aware, however, that some of these approximations are not always accurate and that it is more reliable to compute penetration factors directly from numerical values of the Coulomb wave functions (Appendix A.3). The energy dependence of the s-wave penetration factor at low energies compared to the Coulomb barrier height ($E \ll V_C$) is given by Eqs. (2.124) and (2.125). For higher orbital angular momenta, the charged-particle penetration factors behave at low energies as $P_\ell(E) \sim \exp\left[-a/\sqrt{E} - b\ell(\ell+1)\right]$ (Problem 2.2), where the first exponential term represents the Gamow factor.

Numerical values for the factors P_ℓ and S_ℓ are displayed in Fig. 2.21 for ^{12}C + p and ^{12}C + n in order to illustrate some important points. The curves are obtained by using a radius of $R = 1.25(12^{1/3}+1) = 4.1$ fm. The different energy dependences of P_ℓ for protons and neutrons is striking. The penetration factors for both protons and neutrons drop for decreasing energy, but the former values drop significantly faster since the Coulomb barrier has to be penetrated in addition to the centripetal barrier (for $\ell > 0$). The energy dependence of P_ℓ is similar for protons of all ℓ values, while for neutrons the energy dependence varies for different ℓ values. At higher energies ($E \approx 3$ MeV) we obtain $P_\ell \approx 1$ for protons and neutrons. Note that the curve for the s-wave ($\ell = 0$) penetration factor of ^{12}C + n is simply given by $P_0 = kR$ (see earlier). The shift factors vary far less with energy compared to the penetration factors. In fact, for both neutrons and protons, S_ℓ is almost constant below an energy of a few hundred keV. Of course, one finds $S_0 = 0$ for neutrons as already noted above.

The straight lines for $P_\ell(E)$ at low neutron energies in the log–log plot of Fig. 2.21 are a consequence of the energy dependence $P_\ell(E) \sim E^{\ell+1/2}$. The slopes of the curves are equal to $\ell + 1/2$ since $\log P_\ell(E) \sim \log E^{\ell+1/2} = (\ell+1/2)\log E$. A similar procedure can be applied to charged particles. A graphic illustration of the energy dependence of the penetration factors for ^{12}C + p is given in Fig. 2.22. Since we have $\log P_\ell(E) \sim -a/\sqrt{E} - b\ell(\ell+1)$, straight lines are obtained at low energies when $\log P_\ell(E)$ is plotted versus $-1/\sqrt{E}$. The slopes are similar at low energies where they are determined by the tunneling probability through the Coulomb barrier, while the intercepts depend on the value of ℓ. The straight lines shown in Fig. 2.22 represent a useful tool when checking or interpolating values of $P_\ell(E)$ that are obtained numerically from computer codes.

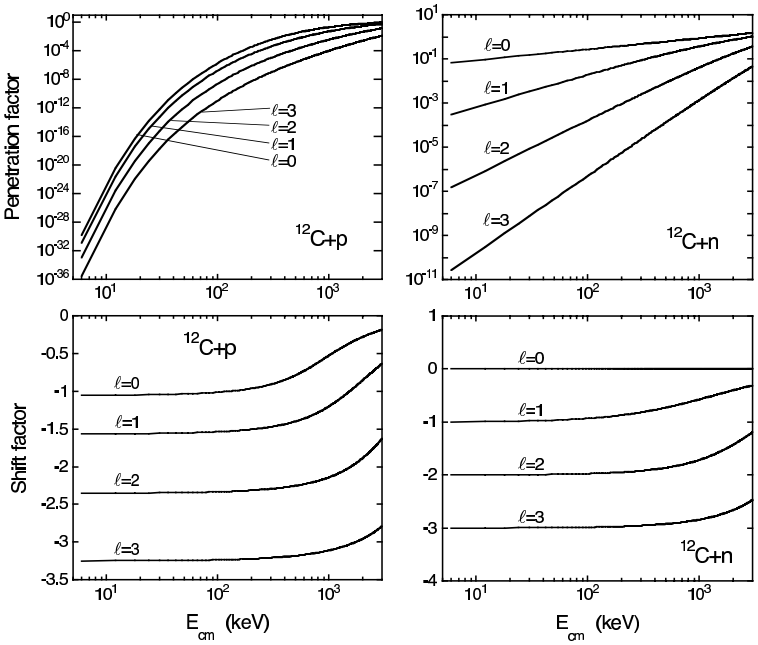

Fig. 2.21 Penetration (top) and shift factors (bottom) for ^{12}C + p (left) and ^{12}C + n (right). In each panel, the curves show the results for orbital angular momenta of ℓ = 0, 1, 2, and 3. All curves are calculated for a radius of $R = 1.25(12^{1/3} + 1)$ = 4.1 fm. The much stronger energy dependence of the penetration factor for protons compared to neutrons is apparent.

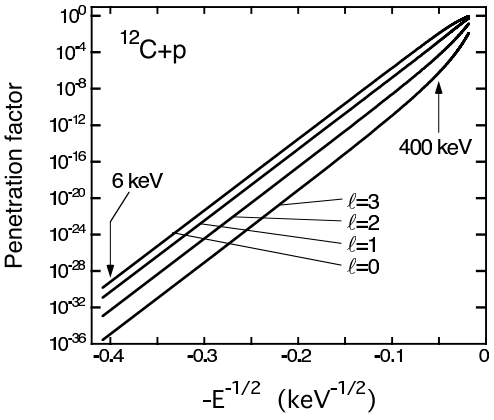

Fig. 2.22 Penetration factor versus $-1/\sqrt{E}$ for the ^{12}C + p reaction. At low energies compared to the Coulomb barrier height ($E \ll V_C$), straight lines are obtained for each value of ℓ.

Up to now we have not specified the reaction channel. Suppose that there are only two channels open for the resonance λ of interest, channel α and channel β. According to Eq. (2.163), the reaction cross sections near resonance in channels α and β are given by

$$\sigma_{\alpha,\mathrm{re},\ell} = (2\ell+1)\frac{\pi}{k_\alpha^2}\frac{\Gamma_{\lambda\alpha}\Gamma_{\lambda\mathrm{r}\alpha}}{(E_\alpha - E_{r\alpha})^2 + (\Gamma_{\lambda\alpha}+\Gamma_{\lambda\mathrm{r}\alpha})^2/4} = \sigma_{(\alpha,\beta)} \tag{2.168}$$

$$\sigma_{\beta,\mathrm{re},\ell} = (2\ell+1)\frac{\pi}{k_\beta^2}\frac{\Gamma_{\lambda\beta}\Gamma_{\lambda\mathrm{r}\beta}}{[(E_\alpha+Q)-(E_{r\alpha}+Q)]^2 + (\Gamma_{\lambda\beta}+\Gamma_{\lambda\mathrm{r}\beta})^2/4} = \sigma_{(\beta,\alpha)} \tag{2.169}$$

It follows directly from the reciprocity theorem, $k_\alpha^2\sigma_{(\alpha,\beta)} = k_\beta^2\sigma_{(\beta,\alpha)}$ (see Eq. (2.13)), that the reaction width of the (α,β) reaction is equal to the entrance channel width of the (β,α) reaction, and vice versa.

2.5.5 *R*-Matrix Theory

It is important to summarize the assumptions we made in the derivation of the reaction cross section formula (see Eq. (2.163)): (i) the spins of the interacting nuclei are zero, (ii) the nucleus has a sharp radius, and (iii) a specific resonance corresponds to a logarithmic derivative of zero at the nuclear boundary. In the formal theory of resonance reactions (*R*-matrix theory) all of these assumptions are relaxed. We will not derive the formalism in any detail (see, for example, Breit 1959, or Lane and Thomas 1958) but will instead present some of the main results. We are specifically interested in the application of the general theory to the case of a single and isolated resonance. As will be seen, the main physical ideas of the formalism developed so far will not change in the formal theory.

Consider again Eq. (2.149), but in order to describe the simplest possible case we will assume that elastic scattering is the only allowed process ($q = 0$). In that case

$$f_0 = (E - E_\lambda)\left(\frac{\partial f_0}{\partial E}\right)_{E_\lambda, q=0} \tag{2.170}$$

By using the definitions of the logarithmic derivative f_0 (see Eq. (2.130)) and of the reduced width $\gamma_{\lambda\mathrm{e}}^2$ (see Eq. (2.159)) we find near a particular level energy E_λ

$$\frac{1}{f_0} = \frac{1}{R}\left(\frac{u_{\mathrm{in}}(r)}{du_{\mathrm{in}}(r)/dr}\right)_{r=R} = \frac{(\partial f_0/\partial E)^{-1}_{E_\lambda,q=0}}{E - E_\lambda} = \frac{\gamma_{\lambda\mathrm{e}}^2}{E_\lambda - E} \equiv \Re \tag{2.171}$$

The quantity $\Re$ is called *R-function*. When the energy E is not close to E_λ, the *R*-function is obtained by summing over all resonances λ. In general,

elastic scattering will not be the only possible process, but other channels are present as well. In order to take these into account, the R-function becomes the *R-matrix*,

$$\Re_{c'c} = \sum_{\lambda} \frac{\gamma_{\lambda c'}\gamma_{\lambda c}}{E_\lambda - E} \tag{2.172}$$

Physically, the R-matrix relates the value of the wave function in the internal region to its derivative at each channel entrance. The above equation gives the energy dependence of the R-matrix explicitly in terms of the energy-independent parameters $\gamma_{\lambda c}$ and E_λ. The poles of the R-matrix, that is, the energies E_λ, are real and hence each of the elements $\Re_{c'c}$ represents a real number. Furthermore, the energies E_λ are independent of the channels c and c'. In other words, the poles of every matrix element $\Re_{c'c}$ occur at the same energies E_λ.

We need to be more precise when defining a *reaction channel* c. The quantity c denotes a set of quantum numbers $\{\alpha(I_1 I_2)s\ell, JM\}$ with

$\alpha(I_1 I_2)$	a specific pair of nuclei 1 and 2, with spins of I_1 and I_2, in a specific state of excitation (thus an excited state of 1 or 2 would correspond to a different α)
$\vec{s} = \vec{I}_1 + \vec{I}_2$	channel spin, with $\lvert I_1 - I_2\rvert \leq s \leq I_1 + I_2$
ℓ	orbital angular momentum
$\vec{J}, M$	total spin and its component, with $\vec{J} = \vec{s} + \vec{\ell}$

For the entrance channel consisting of a projectile and a target nucleus, we set $\vec{I}_1 = \vec{j}_p$ and $\vec{I}_2 = \vec{j}_t$. Conservation of the total angular momentum restricts the possible J values of the resonance which can be populated in the reaction to (Appendix B)

$$\vec{J} = \vec{\ell} + \vec{j}_p + \vec{j}_t \tag{2.173}$$

Each of these spins has $(2I + 1)$ orientations in space, which are determined by the magnetic quantum number $m_I = 0, 1, \ldots, \pm I$. Thus there are $(2\ell + 1)(2j_p + 1)(2j_t + 1)$ different sets of spin orientations, corresponding to different quantum states of the system. For an unpolarized beam and target, each such state has the same probability, that is $[(2\ell + 1)(2j_p + 1)(2j_t + 1)]^{-1}$. Therefore, the cross section has to be multiplied by the relative probability that the unpolarized projectiles and target nuclei will be found to have a total spin of J, which is given by

$$g(J) = \frac{2J + 1}{(2j_p + 1)(2j_t + 1)(2\ell + 1)} \tag{2.174}$$

From the R-matrix, the cross sections and phase shifts can be derived for any number of resonances and channels (Lane and Thomas 1958). In the following, we will only focus on a particularly simple but useful case, that is, the reaction cross section near an isolated resonance λ of spin J. The one-level, many channel approximation of R-matrix theory (or generalized one-level Breit–Wigner formula) for the cross section of a reaction (α,α'), involving charged or neutral particles with projectile and target spins of j_p and j_t, is given by

$$\sigma_{\mathrm{re}}(\alpha,\alpha') = \frac{\pi}{k^2}\frac{2J+1}{(2j_p+1)(2j_t+1)}\frac{\left(\sum\limits_{\ell s}\Gamma_{\lambda c}\right)\left(\sum\limits_{\ell' s'}\Gamma_{\lambda c'}\right)}{(E-E_\lambda-\Delta_\lambda)^2+\Gamma_\lambda^2/4} \tag{2.175}$$

with

$$\Gamma_{\lambda c}(E) = 2P_c(E)\gamma_{\lambda c}^2 \qquad \text{(particle width)} \tag{2.176}$$

$$\Gamma_\lambda(E) = \sum_{c''}\Gamma_{\lambda c''}(E) \qquad \text{(total width)} \tag{2.177}$$

$$\Delta_\lambda(E) = \sum_{c''}\Delta_{\lambda c''}(E) \qquad \text{(total level shift)} \tag{2.178}$$

$$\Delta_{\lambda c}(E) = -[S_c(E)-B_c]\gamma_{\lambda c}^2 \qquad \text{(partial level shift)} \tag{2.179}$$

$$\beta(E) = \arctan\frac{\Gamma_\lambda(E)}{2[E_\lambda - E + \Delta_\lambda(E)]} \qquad \text{(resonance elastic scattering phase shift)} \tag{2.180}$$

The parameter B_c will be described later. The penetration and shift factors refer to the nuclear radius. In principle, one can chose an arbitrary radius beyond the range of the nuclear force so that the external wave functions reflect the solutions of the wave equation containing only the Coulomb interaction. However, it is also desirable to chose R as small as possible so that the characteristic quantities of the resonance theory contain primarily information concerning the nuclear interaction. Commonly, the interaction radius R is the smallest separation distance of the nuclear pair at which the nuclear potential is negligible. This radius is customarily chosen in R-matrix theory as $R = r_0(A_t^{1/3} + A_p^{1/3})$, with a radius parameter in the range of r_0 = 1.0–1.5 fm.

The above expression for the reaction cross section (see Eq. (2.175)) contains certain complications with respect to practical applications. This comes about because, in general, the energy dependence of the penetration and shift factor has to be taken into account. The quantity P_c is strongly energy dependent, but the energy dependence of S_c is weak (Fig. 2.21). The usual approximation procedure, called the *Thomas approximation* (Thomas 1951), is to expand the level shift linearly with respect to energy. We call the energy at which the cross section $\sigma_{\mathrm{re}}(\alpha,\alpha')$ has a maximum the *observed resonance energy* E_r. It is

defined by the requirement

$$E_r - E_\lambda - \Delta_\lambda(E_r) = 0 \tag{2.181}$$

The boundary condition parameter B_c in Eq. (2.179), defined as the real and arbitrary value of the logarithmic derivative of the radial wave function in channel c at the radius R, determines the eigenvalues E_λ (in previous sections, we used implicitly the zero derivative condition, $B_c = 0$). It is customarily chosen as $B_c = S_c(E_r)$ so that the level shift Δ at the observed resonance energy E_r becomes zero,

$$\Delta_{\lambda c}(E_r) = -[S_c(E_r) - S_c(E_r)]\gamma_{\lambda c}^2 = 0 \qquad \text{and} \qquad E_r = E_\lambda \tag{2.182}$$

With the expansion

$$\Delta_\lambda(E) \approx \Delta_\lambda(E_r) + (E - E_r)\left(\frac{d\Delta_\lambda}{dE}\right)_{E_r} \tag{2.183}$$

we obtain by using Eq. (2.181)

$$E_\lambda + \Delta_\lambda - E \approx E_r - E + (E - E_r)\left(\frac{d\Delta_\lambda}{dE}\right)_{E_r} = (E_r - E)\left[1 - \left(\frac{d\Delta_\lambda}{dE}\right)_{E_r}\right] \tag{2.184}$$

Substitution into Eq. (2.175) yields

$$\sigma_{\text{re}}(\alpha, \alpha') = \frac{\pi}{k^2}\frac{2J+1}{(2j_p+1)(2j_t+1)}\frac{\left(\sum_{\ell s}\Gamma_{\lambda c}\right)\left(\sum_{\ell' s'}\Gamma_{\lambda c'}\right)}{(E_r - E)^2[1 - (d\Delta_\lambda/dE)_{E_r}]^2 + \Gamma_\lambda^2/4}$$

Dividing the numerator and denominator by $[1 - (d\Delta_\lambda/dE)_{E_r}]^2$ gives

$$\sigma_{\text{re}}(\alpha, \alpha') = \frac{\pi}{k^2}\frac{2J+1}{(2j_p+1)(2j_t+1)}\frac{\left(\sum_{\ell s}\Gamma^o_{\lambda c}\right)\left(\sum_{\ell' s'}\Gamma^o_{\lambda c'}\right)}{(E_r - E)^2 + (\Gamma^o_\lambda)^2/4} \tag{2.185}$$

where the "observed" widths $\Gamma^o_{\lambda i}$ are given in terms of the previously defined "formal" widths $\Gamma_{\lambda i}$ (see Eq. (2.176)) by

$$\Gamma^o_{\lambda c} \equiv \frac{\Gamma_{\lambda c}}{1 - (d\Delta_\lambda/dE)_{E_r}} = \frac{\Gamma_{\lambda c}}{1 + \left(\sum_{c''}\gamma^2_{\lambda c''}\frac{dS_{c''}}{dE}\right)_{E_r}} \tag{2.186}$$

The main advantage of using Eq. (2.185) compared to Eq. (2.175) is that the complication of an energy-dependent shift factor in the denominator is absent.

Since the former expression has a simpler (Lorentzian) structure, it is used in the vast majority of applications. However, we had to introduce a new quantity. The reader must be careful when applying Eq. (2.185) in the analysis of experimental data. It has to be understood that the partial widths thus obtained represent "observed" widths. As can be seen from Eq. (2.186), the difference between "observed" and "formal" partial width may be substantial for levels with a large reduced width. We can also introduce an "observed" reduced width by writing

$$\Gamma_{\lambda c}^{o} = \frac{2P_c(E)\gamma_{\lambda c}^2}{1 + \left(\sum_{c''} \gamma_{\lambda c''}^2 \frac{dS_{c''}}{dE}\right)_{E_r}} = 2P_c(E)(\gamma_{\lambda c}^{o})^2 \tag{2.187}$$

As a general guide, partial widths have to be interpreted as "observed" quantities whenever a Lorentzian structure is assumed for the cross section (for example, in reaction rate calculations, mean lifetime measurements, or thick target yields).

Finally, we express the resonance phase shift and its energy derivative in terms of the "observed" total width. We obtain from Eqs. (2.180) and (2.184) immediately

$$\beta = \arctan \frac{\Gamma_\lambda / [1 - (d\Delta_\lambda / dE)_{E_r}]}{2(E_r - E)} = \arctan \frac{\Gamma_\lambda^o}{2(E_r - E)} \tag{2.188}$$

and, similar to Eq. (2.158),

$$\left(\frac{d\beta}{dE}\right)_{E_r} = \frac{2}{(\Gamma_\lambda^o)_{E_r}} \tag{2.189}$$

This expression is frequently used in calculations of "observed" particle partial widths (see Section 2.5.7).

2.5.6
Experimental Tests of the One-Level Breit–Wigner Formula

The total cross section for neutrons incident on a target consisting of a natural isotopic mixture of cadmium is shown in Fig. 2.23. The data are fitted by a one-level Breit–Wigner formula, superimposed on a $1/v$ background (Section 2.6). It is obvious that the agreement with the data is extremely accurate. The Breit–Wigner formula describes reliably the shape of resonances if their widths are small compared to their energy separation.

The resonance reaction theory developed so far does not only apply to unbound states, but to bound states as well. In the latter case, the Breit–Wigner formula allows for the calculation of the cross section wing of a *subthreshold resonance* (Example 2.1). The Breit–Wigner formula has important applications

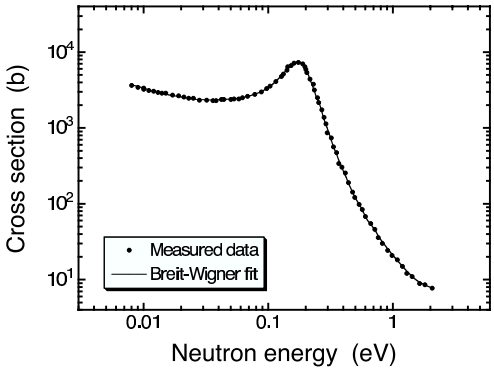

Fig. 2.23 Total cross section for neutrons incident on a target consisting of a natural isotopic mixture of cadmium. The data are fitted by a one-level Breit–Wigner formula, superimposed on a $1/v$ background. The deduced resonance parameters are E_λ = 0.176 eV, Γ = 0.115 eV, and $\sigma_{\max}$ = 7.2×10^{-21} cm^2. The Breit–Wigner formula reproduces the shape of resonances accurately if their widths are small compared to their energy separation. Reprinted with permission from H. H. Goldsmith, H. W. Ibser and B. T. Feld, Rev. Mod. Phys., Vol. 19, p. 259 (1947). Copyright (1947) by the American Physical Society.

in nuclear astrophysics, especially in cases where the cross section of interest cannot be measured directly and has to be estimated theoretically. For example, consider the following situation which is frequently encountered in practice. Data have been obtained in some higher lying bombarding energy range. The energy range of interest for stellar fusion, however, is located outside the range for which data have been measured. By fitting the existing data to a Breit–Wigner formula, one obtains the resonance energy and widths as phenomenological parameters which are then used to extrapolate the cross section to the energy region of interest.

Frequently, the widths of astrophysically important resonances are rather small (less than a few eV) and it is experimentally no longer feasible to measure the cross section directly at specific energies near the resonance. What is directly measured in such cases is the integral under the resonance cross section curve. The Breit–Wigner formula provides an accurate equation for integrating the resonance cross section, resulting in convenient analytical expressions for narrow-resonance reaction rates (Section 3.2.4) and thick-target yields (Section 4.8.1).

The total cross section for several overlapping resonances of different spins and parities can be described by an incoherent sum of one-level Breit–Wigner formulas. If two resonances have the same J^π value, however, they may interfere and the resulting expressions become more complicated. Also, the differential cross sections of two broad resonances may interfere even if their J^π values are different.

It must be emphasized again that the resonance theory described here is not capable of predicting resonance energies and widths. These quantities are treated as phenomenological parameters. Absolute cross sections can only be obtained either by fitting resonance data, or if the resonance energies and partial (or reduced) widths are independently known from other sources (Section 2.5.7). In the following numerical example, the one-level Breit–Wigner formula will be applied to a subthreshold resonance.

Example 2.1

The Q-value of the ^{20}Ne(p,γ)^{21}Na reaction amounts to Q = 2431.3 keV. The ^{21}Na level at E_x = 2425 keV ($J^\pi = 1/2^+$) is located just below the proton threshold and corresponds to a subthreshold s-wave ($\ell = 0$) resonance at a center-of-mass energy of $E_r = -6.4$ keV (Fig. 2.24a). The (formal) reduced proton width for this level can be obtained from (d,n) proton transfer reaction measurements (Terakawa et al. 1993). The value is $\gamma^2_{\mathrm{p},\ell=0} = 1.41 \times 10^6$ eV. The E_x = 2425 keV level decays to the ground state with a probability (branching ratio) of 1 (100%) via emission of M1/E2 radiation (Appendix B). The value of the (formal) γ-ray partial width at E_r, obtained from the measured mean lifetime of the state (Anttila, Keinonen and Bister 1977), amounts to $\Gamma_\gamma(E_r)$ = 0.30 eV. Calculate the contribution of this level to the astrophysical S-factor (the S-factor is defined in Section 3.2.1) versus bombarding energy below 2 MeV.

In this case only two channels are open. The level can decay via emission of either a proton or a γ-ray. We may write the Breit–Wigner formula (see Eq. (2.175)) as

$$\sigma_{^{20}\mathrm{Ne+p}}(\mathrm{p},\gamma) = \frac{\pi}{k^2}\frac{2J+1}{(2j_p+1)(2j_t+1)}\frac{\Gamma_{\mathrm{p},\ell=0}\Gamma_{\gamma,\mathrm{M1/E2}}}{(E-E_\lambda-\Delta_\lambda)^2+(\Gamma_{\mathrm{p},\ell=0}+\Gamma_{\gamma,\mathrm{M1/E2}})^2/4}$$

The cross section has a maximum at the observed resonance energy $E_r = E_\lambda + \Delta_\lambda(E_r) = E_\lambda$ (see Eqs. (2.181) and (2.182)) since we chose the boundary condition as $\Delta_\lambda(E_r) = 0$. Therefore, we set $E_\lambda = -6.4$ keV. We find the energy-dependent proton width from the expression $\Gamma_{\mathrm{p},\ell=0}(E) = 2P_{\ell=0}(E)\gamma^2_{\mathrm{p},\ell=0}$ (see Eq. (2.176)). The energy dependence of the γ-ray partial width is given by $\Gamma_{\gamma,L} \sim E_\gamma^{2L+1}$ (see Eq. (1.21)), with E_γ the γ-ray energy and L the γ-ray multipolarity. The M1/E2 multipolarity mixing ratio (see Eq. (1.31)) for this level is not known. It is sufficient to assume here that the transition to the ground state ($E_f = 0$) proceeds via pure M1 emission. Thus

$$\frac{\Gamma_{\gamma,\mathrm{M1}}(E)}{\Gamma_{\gamma,\mathrm{M1}}(E_r)} = \left[\frac{E_\gamma(E)}{E_\gamma(E_r)}\right]^{2L+1} = \left[\frac{E+Q-E_f}{E_r+Q-E_f}\right]^{2L+1} = \left[\frac{E+Q}{E_r+Q}\right]^3$$

The influence of the γ-ray channel on the level shift can be neglected. From Eqs. (2.178) and (2.179) one finds

$$\Delta_\lambda(E) \approx \Delta_{\mathrm{p},\ell=0}(E) = -[S_{\ell=0}(E) - S_{\ell=0}(E_r)]\gamma^2_{\mathrm{p},\ell=0}$$

We obtain from the definition of the astrophysical S-factor (see Eq. (3.70))

$$\begin{aligned} S_{^{20}\mathrm{Ne+p}}(\mathrm{p},\gamma) &= E\, e^{2\pi\eta}\sigma_{^{20}\mathrm{Ne+p}}(p,\gamma) \\ &= \frac{E e^{2\pi\eta}\frac{\pi}{k^2}\frac{2J+1}{(2j_p+1)(2j_t+1)}2P_{\ell=0}(E)\gamma^2_{\mathrm{p},\ell=0}\Gamma_{\gamma,\mathrm{M1}}(E_r)\left(\frac{E+Q}{E_r+Q}\right)^3}{\left\{E - E_r + [S_{\ell=0}(E) - S_{\ell=0}(E_r)]\gamma^2_{\mathrm{p},\ell=0}\right\}^2 + [\Gamma(E)]^2/4} \end{aligned}$$

with $\Gamma(E) = \Gamma_{\mathrm{p},\ell=0}(E) + \Gamma_{\gamma,\mathrm{M1}}(E)$. Numerically we find (with E in MeV and M_i in u)

$$\begin{aligned} 2\pi\eta &= 0.989534\, Z_p Z_t \sqrt{\frac{1}{E}\frac{M_t M_p}{M_t + M_p}} \\ E\frac{\pi}{k^2} &= 6.56618216 \times 10^{-1}\frac{M_t + M_p}{M_t M_p} \qquad (\mathrm{MeV\,b}) \\ \frac{2J+1}{(2j_p+1)(2j_t+1)} &= \frac{2\cdot\frac{1}{2}+1}{\left(2\cdot\frac{1}{2}+1\right)(2\cdot 0+1)} = 1 \\ S_{\ell=0}(E_r) &= -1.537 \end{aligned}$$

The penetration and shift factors are directly computed from the Coulomb wave functions (see Eq. (2.162)). The resulting calculated S-factor for the ground-state transition in the ^{20}Ne(p,γ)^{21}Na reaction is shown as a solid line in Fig. 2.24b. The data points display the experimental S-factor. These results represent one of the very few examples in nuclear physics where a tail of a subthreshold resonance is observed without interference from unbound states or direct radiative capture.

It must be emphasized that the solid line does not represent a fit to the data. It is calculated by using the Breit–Wigner formula with parameters (resonance energy, proton and γ-ray partial widths) that are obtained from independent experiments (that is, *not* from capture measurements). It should also be noted that the total width at the resonance energy amounts to $\Gamma(E_r) = \Gamma_\gamma(E_r)$ =0.3 eV. In other words, the S-factor is extrapolated over 1500 keV / 0.3 eV = 5×10^6 resonance widths. The agreement between experiment and calculation is remarkable and provides strong support for the applicability of the Breit–Wigner formula to isolated resonances.

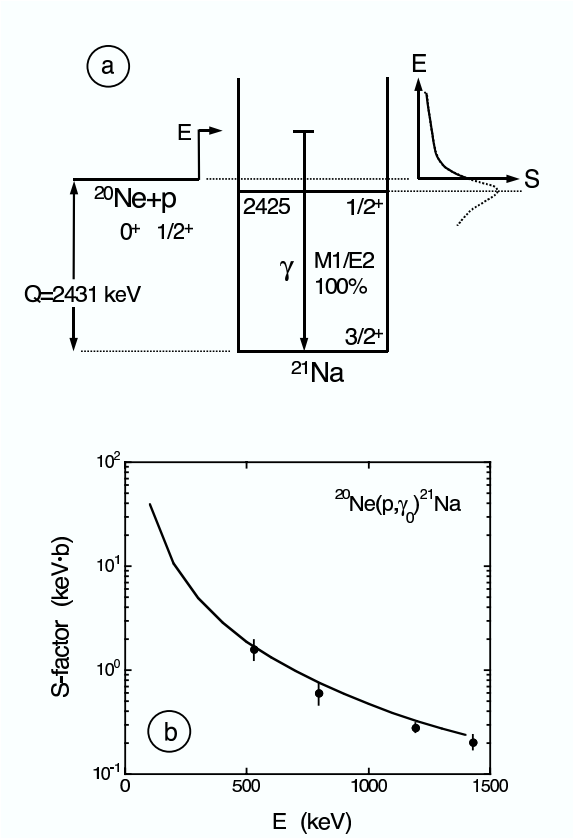

Fig. 2.24 (a) Level scheme of ^{21}Na showing a subthreshold s-wave ($\ell = 0$) resonance in ^{20}Ne + p, corresponding to a level at E_x = 2425 keV ($J^\pi = 1/2^+$) which is located just below the proton threshold. (b) Astrophysical S-factor of the ^{20}Ne(p,γ)^{21}Na reaction versus center-of-mass proton energy for the γ-ray transition to the ground state of ^{21}Na. The data points display the measured S-factor (from Rolfs and Rodney 1975), while the solid line shows the result of the calculation explained in the text. Note that the solid line is not a fit to the data. The agreement between data and calculation is remarkable since the Breit–Wigner formula had to be extrapolated over more than 10^6 resonance widths.

2.5.7 Partial and Reduced Widths

We have seen how the resonance cross section can be expressed in terms of resonance energies and reduced widths. For some reactions, however, no cross section data are available. In such cases it becomes important to estimate the cross section theoretically. The Breit–Wigner formula can only be used for this purpose if the resonance energies and reduced widths are known from independent sources (see Example 2.1).

Resonances that are generated by simple explicit potentials are discussed in Section 2.4. Such *single-particle resonances* are generally broad at higher bombarding energies and their energy separation is large. In contrast to these, many measured resonances are very narrow and their spacing is small (Fig. 2.19). These resonances could not be explained by single-particle potentials and it was therefore necessary to develop a theory of resonances without reference to a specific nuclear potential (Section 2.5.1). The reduced widths depend on, as yet unknown, properties of the nuclear interior and are treated as phenomenological parameters.

According to Bohr (1936), the observed resonances correspond to virtual states in the nucleus. These virtual states are not single-particle levels, but are the result of the interactions of many nucleons. This many-nucleon picture is also referred to as *compound nucleus description*. The close spacing of the observed resonances is then explained by the fact that there are many different ways by which a large number of nucleons can be excited. The observed resonances are then caused by the rapid variation of the total nuclear wave function of the target-plus-projectile system with energy. In the following we will develop this picture quantitatively. Our goal will be to relate the reduced widths to nuclear properties which can be estimated by using models of nuclear structure.

Consider the total wave function of the target-plus-projectile system, Ψ, with $H\Psi = E\Psi$. The total Hamiltonian H, although unknown, may be written as

$$\begin{aligned} H &= H_\xi^t + E_K^p(r) + \sum_{i=1}^{A} V_i(\xi_i, x) \\ &= \left[H_\xi^t + E_K^p(r) + \overline{V}(r)\right] + \left[-\overline{V}(r) + \sum_{i=1}^{A} V_i(\xi_i, x)\right] = H_0 + H' \end{aligned} \tag{2.190}$$

with H_ξ^t the Hamiltonian of the target nucleus consisting of A nucleons, $E_K^p(r)$ the kinetic energy of the projectile, $V_i(\xi_i, x)$ the interactions between each target nucleon with the projectile, and $\overline{V}(r)$ an average potential of the projectile in the field of the target nucleus. The quantity H_0 is the single-particle Hamiltonian, and H' describes the *residual interaction* (that is, the deviation from an average potential). Without the residual interaction, the potential $\overline{V}(r)$ would give rise to single-particle resonances, corresponding to single-particle levels in the target-plus-projectile system. However, the quantity H' causes the single-particle levels to split into a large number of distinct levels. Each of these states corresponds to a complicated mixture of configurations and is described by a complicated sum of wave functions. Consequently, the logarithmic derivative of the radial wave function at the nuclear boundary, that is, the reduced width $\gamma_{\lambda c}^2$, will in general be different for each virtual state.

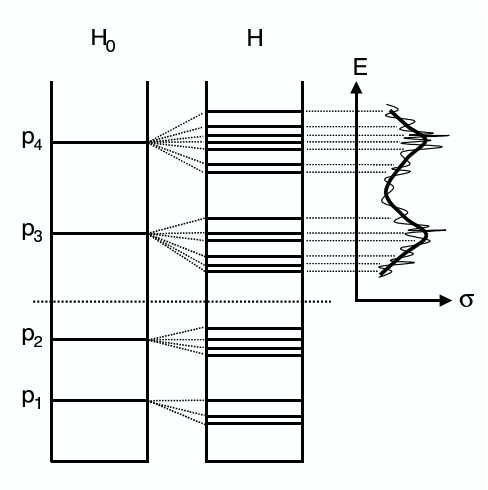

Fig. 2.25 Level scheme and cross section versus energy. A single-particle Hamiltonian H_0 generates the single-particle levels p_1, p_2, p_3, p_4. The actual Hamiltonian H gives rise to a splitting of each single-particle level into many actual states. The latter show up as a fine structure in the cross section versus energy curve. See the text.

Such levels which are described by the configurations of many nucleons are referred to as *compound-nucleus levels*.

The situation is shown schematically in Fig. 2.25. The single-particle Hamiltonian H_0 gives rise to the single-particle levels p_1, p_2, p_3, p_4. The levels p_1 and p_2 are bound states. The actual Hamiltonian H causes a splitting of each single-particle level into many actual states. These can be observed as resonances in the cross section (thin solid line). However, the single-particle character does not get entirely lost. If the measured cross section curve is averaged over the observed fine structure, then the single-particle resonances are approximately recovered (thick solid line). We may also say that, in this picture, each reduced width $\gamma_{\lambda c}^2$ of an actual level belongs to a definite single-particle level p_i. The entire set of reduced widths can then be split up into groups, each group corresponding to a definite value of p_i.

In the following, we will consider the simple case of only one open nucleon channel (elastic only) for compound nucleus formation or decay. It is useful at this point to express the particle width in a different way. We have seen that Γ_λ corresponds to the total width of a resonance λ, or the total width of a virtual level in the compound nucleus. A finite level width, in turn, implies a finite mean lifetime τ of the level, since $\Gamma_\lambda \tau_\lambda \approx \hbar$. Therefore, we can identify $1/\tau_\lambda \approx \Gamma_\lambda/\hbar$ with the decay (or formation) probability of the level per unit time. A partial width $\Gamma_{\lambda c}$ corresponds then to the decay (or formation) probability of

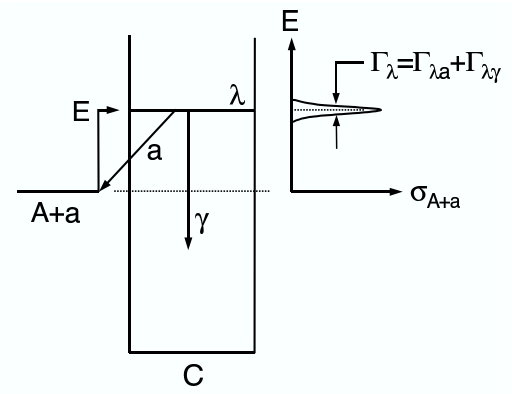

Fig. 2.26 Level scheme of compound nucleus C showing a single unbound (or virtual) state λ which may decay by emission of particles (a) or photons (γ). The full width at half maximum (FWHM) of the resonance in the cross section versus energy curve corresponds to the total width Γ_λ which is equal to the sum of all partial widths. The latter quantities are a measure for the decay (or formation) probability of level λ through a particular channel c.

level λ through a particular channel c. The decay of a compound nucleus state into two channels is shown schematically in Fig. 2.26.

The partial width $\Gamma_{\lambda c}$ will now be determined from the flux of the particles through the only open channel c. The probability per unit time, $\Gamma_{\lambda c}/\hbar$, for the emission of a particle is given by the number of particles per second leaving the channel. This number can be calculated by integrating the current (see Eq. (2.45)) through a sphere of radius R over the full solid angle,

$$\frac{\Gamma_{\lambda c}}{\hbar} = \int_{d\Omega} R^2 j \, d\Omega = \int_{d\Omega} R^2 \frac{\hbar}{2mi} \left(\psi^* \frac{\partial \psi}{\partial r} - \frac{\partial \psi^*}{\partial r} \psi \right)_{r=R} d\Omega \tag{2.191}$$

With $\psi = Y(\theta,\phi)R_c(r) = Y(\theta,\phi)u_c(r)/r$ (Appendix A) we find

$$\begin{aligned} \frac{\Gamma_{\lambda c}}{\hbar} &= \frac{\hbar}{2mi} \int_{d\Omega} R^2 \left[\frac{u_c^*}{r} \frac{d}{dr} \left(\frac{u_c}{r} \right) - \frac{u_c}{r} \frac{d}{dr} \left(\frac{u_c^*}{r} \right) \right]_{r=R} |Y|^2 \, d\Omega \\ &= \frac{\hbar}{2mi} \int_{d\Omega} R^2 \frac{1}{R^2} \left(u_c^* \frac{du_c}{dr} - u_c \frac{du_c^*}{dr} \right)_{r=R} |Y|^2 \, d\Omega \end{aligned} \tag{2.192}$$

The radial wave function u_c of the compound state can be expanded in terms of single-particle radial eigenfunctions u_{pc}, which form a complete set of orthonormal functions. The eigenfunctions u_{pc} describe a single nucleon moving in a single-particle potential. We may write

$$u_c(R) = \sum_p A_{\lambda pc} u_{pc}(R) \tag{2.193}$$

The above discussion of compound levels implies that, at a given energy, one particular single-particle state p contributes mainly to the width of level λ. This means that for a given level λ one of the terms in the sum of Eq. (2.193) is much larger than the others. Hence

$$u_c(R) \approx A_{\lambda pc} u_{pc}(R) \tag{2.194}$$

By using the normalization of the spherical harmonic Y and the definition of the logarithmic derivative, $f_{pc}(E) = R(u_{pc}^{-1}\, du_{pc}/dr)_{r=R}$ (see Eq. (2.130)), we obtain from Eqs. (2.192) and (2.194)

$$\begin{aligned}\Gamma_{\lambda c} &= \frac{\hbar^2}{2mi} A_{\lambda pc}^2 \left(u_{pc}^* \frac{du_{pc}}{dr} - u_{pc} \frac{du_{pc}^*}{dr} \right)_{r=R} \\ &= \frac{\hbar^2}{2miR} A_{\lambda pc}^2 \left(u_{pc}^* u_{pc} f_{pc} - u_{pc} u_{pc}^* f_{pc}^* \right)_{r=R} = \frac{\hbar^2 |u_{pc}(R)|^2}{2miR} A_{\lambda pc}^2 (f_{pc} - f_{pc}^*)\end{aligned} \tag{2.195}$$

Since we describe a decaying compound state, the radial wave function for $r > R$ is given by $u_{pc}(r) = A u_{pc}^+(r)$, that is, we have $B = 0$ for a purely outgoing wave (see Eq. (2.160)). This condition is equivalent to $f_{pc}(E) = S_c + iP_c$ (see Eq. (2.161)). It follows that

$$\Gamma_{\lambda c} = \frac{\hbar^2 |u_{pc}(R)|^2}{2miR} A_{\lambda pc}^2 [(S_c + iP_c) - (S_c - iP_c)] = 2\frac{\hbar^2}{mR^2} P_c A_{\lambda pc}^2 \frac{R}{2} |u_{pc}(R)|^2 \tag{2.196}$$

This can be expressed as

$$\Gamma_{\lambda c} = 2\frac{\hbar^2}{mR^2} P_c\, C^2 S\, \theta_{pc}^2 \tag{2.197}$$

with

$$C^2 S = A_{\lambda pc}^2 \qquad \text{(spectroscopic factor)} \tag{2.198}$$

$$\theta_{pc}^2 = \frac{R}{2} \left| u_{pc}(R) \right|^2 \quad \text{(dimensionless single-particle reduced width)} \tag{2.199}$$

Comparison to Eq. (2.176) shows that the reduced width $\gamma_{\lambda c}^2$ has been reformulated in terms of a constant ($\hbar^2/mR^2$) and the quantities θ_{pc}^2 and C^2S.

Strictly speaking, the quantities S and C^2 denote a spectroscopic factor (Section 1.6.2) and the square of an isospin Clebsch–Gordan coefficient, respectively. The former quantity is frequently calculated using the nuclear shell model (Section 1.6), while the latter depends on the nuclear reaction (see, for example, Brussaard and Glaudemans 1977). In the present context of partial widths, only the product C^2S is of interest. The spectroscopic factor depends

on the many-nucleon structure of level λ and is a measure for the relative probability that an actual compound state λ can be described by the single-particle state p. The structure of Eq. (2.197) emphasizes that the partial width for nucleon emission from a compound level can be thought of as a product of three factors: (i) the probability that the nucleons will arrange themselves in a configuration corresponding to the final state, C^2S, (ii) the probability that the single nucleon will appear at the boundary, $|u_{pc}(R)|^2$, and (iii) the probability that the single nucleon will penetrate the Coulomb and angular momentum barriers, P_c. By introducing a single-particle partial width

$$\Gamma_{\lambda pc} = 2\frac{\hbar^2}{mR^2} P_c \theta_{pc}^2 \tag{2.200}$$

we may also express Eq. (2.197) as

$$\Gamma_{\lambda c} = C^2S\, \Gamma_{\lambda pc} \tag{2.201}$$

In other words, the spectroscopic factor can be written as the ratio of the two quantities $\Gamma_{\lambda c}$ and $\Gamma_{\lambda pc}$. Since both of these partial widths are strongly energy dependent through the penetration factor P_c, they have to be calculated at the *same* incident energy E.

It is apparent that there are two different methods of estimating partial widths for nucleon channels once the spectroscopic factor C^2S has been obtained by independent means. If Eq. (2.197) is used, then the penetration factor P_c and the dimensionless single-particle reduced width θ_{pc}^2 must be computed. On the other hand, if Eq. (2.201) is employed, then the single-particle partial width $\Gamma_{\lambda pc}$ has to be calculated. This can be achieved, for example, by solving the Schrödinger equation numerically for the elastic scattering of nucleons by an appropriate single-particle potential (Schiffer 1963, Iliadis 1997). The single-particle partial width is then directly obtained from the slope of the resonance phase shift at the resonance energy (see Eq. (2.189)). The former method is computationally more convenient if values of θ_{pc}^2 are already available.

Numerical values of the dimensionless single-particle reduced width θ_{pc}^2 for protons are reported in Iliadis (1997) (Fig. 2.27) and Barker (1998). The results were obtained by calculating u_{pc} for a Woods–Saxon single-particle potential (Section 1.6.1). The value of θ_{pc}^2 depends on the interaction radius R, the orbital angular momentum ℓ, and the number of nodes of the radial wave function in the nuclear interior. The numerical values shown in Fig. 2.27 have been obtained with $R = 1.25(A_p^{1/3} + A_t^{1/3})$ fm. Obviously, for estimates of $\Gamma_{\lambda c}$ the quantities θ_{pc}^2 and P_c have to be computed at the same radius R. The θ_{pc}^2 values from Iliadis (1997) represent "observed" quantities, while the results from Barker (1998) represent "formal" quantities. Unfortunately, the dimensionless single-particle reduced width θ_{pc}^2 is frequently set equal to unity in the litera-

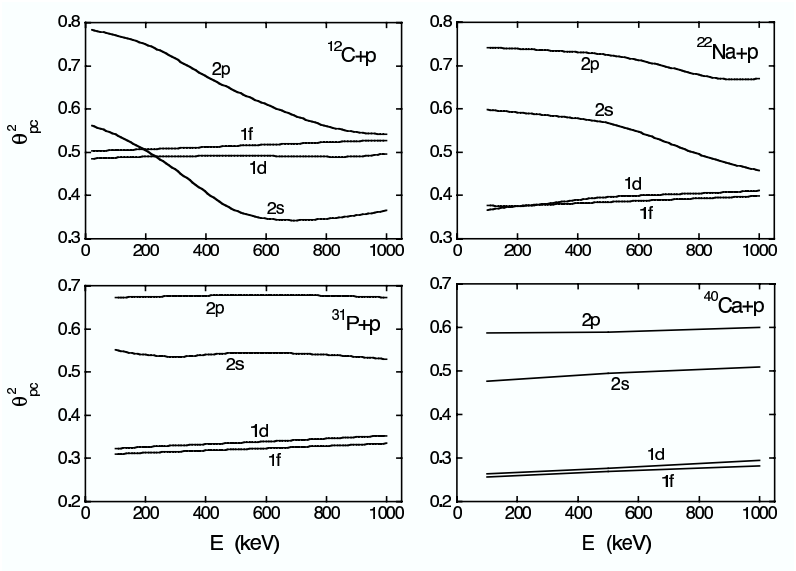

Fig. 2.27 "Observed" dimensionless single-particle reduced width θ^2_{pc} for ^{12}C + p, ^{22}Na + p, ^{31}P + p, and ^{40}Ca + p versus center-of-mass proton energy. In each panel, the curves correspond to different orbital angular momenta (ℓ = 0, 1, 2, and 3) and have been computed for a radius of $R = 1.25(A_p^{1/3} + A_t^{1/3})$ fm. Reprinted from C. Iliadis, Nucl. Phys. A, Vol. 618, p. 166 (1997). Copyright (1997), with permission from Elsevier.

ture. In this case, a significant error is introduced in the estimation of partial widths.

Frequently, a resonance cannot be observed directly. This happens, for example, if the cross section is too small or if the target is radioactive. In such cases, the formalism discussed above can be used to estimate the absolute reaction cross section. Once the spectroscopic factor is either calculated using the nuclear shell model (Section 1.6), or measured using transfer reactions, the particle partial width can be estimated in a straightforward way. The reaction cross section is then obtained by applying the Breit–Wigner formula.

It is interesting to investigate the reliability of Eq. (2.197) for the calculation of proton partial widths. Figure 2.28 shows a comparison of measured and estimated proton partial widths for compound levels in ^{25}Al, ^{27}Al and ^{31}P. The ratio of partial widths, $\Gamma_{\rm exp}/\Gamma_{\lambda c}$, is shown in part (a) versus the value of C^2S, and in part (b) versus the observed resonance energy E_r. The values of $\Gamma_{\lambda c}$ are estimated from Eq. (2.197) by using proton spectroscopic factors measured in (^{3}He,d) transfer reactions and by computing θ^2_{pc} and P_c numerically. The experimental proton widths $\Gamma_{\rm exp}$ were directly measured in resonance elastic

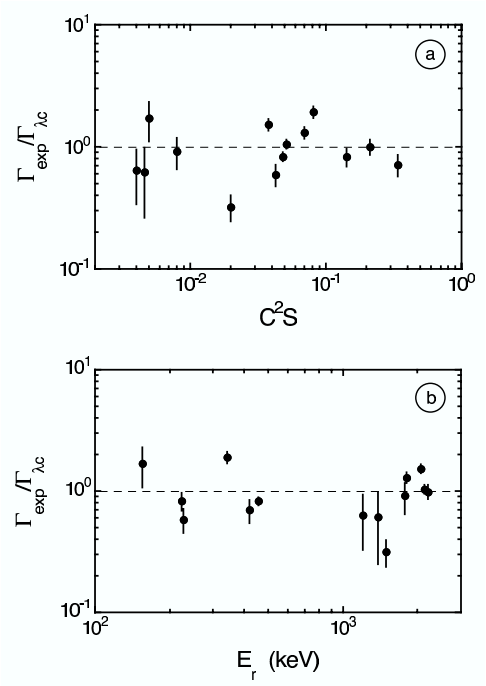

Fig. 2.28 Ratio of measured and estimated proton partial widths, $\Gamma_{\rm exp}/\Gamma_{\lambda c}$, for levels in ^{25}Al, ^{27}Al, and ^{31}P (a) versus the value of C^2S, and (b) versus the observed resonance energy E_r. The experimental proton widths $\Gamma_{\rm exp}$ were directly measured in resonance elastic proton scattering or proton capture reactions. The calculated values $\Gamma_{\lambda c}$ are obtained from Eq. (2.197) by using spectroscopic factors measured in (^{3}He,d) transfer studies.

proton scattering or proton capture reactions. The error bars of the displayed ratios consider only the uncertainties of the experimental proton widths. It can be seen that experimental and estimated proton partial widths agree on average within ≈50%. In fact, we expect that the parametrizations of $\Gamma_{\lambda c}$ (see Eqs. (2.197) and (2.201)) are more accurate than this since we have entirely neglected the errors in the measured transfer spectroscopic factors. Further systematic studies are needed.

Example 2.2

An important resonance in the ^{17}F(p,γ)^{18}Ne reaction occurs at a center-of-mass energy of E_r = 600 keV ($J^\pi = 3^+$). The spectroscopic factors for this resonance are known from independent measurements (that is, neutron-stripping on the mirror target nucleus ^{17}O). Their values are $(C^2S)_{\ell=0}$ = 1.01 and $(C^2S)_{\ell=2} \approx 0$. Estimate the "observed" proton partial width for this resonance.

We write with Eq. (2.197)

$$\begin{aligned}\Gamma^o_{\mathrm{p},\ell=0} &= 2\frac{\hbar^2}{mR^2}\,P_{\ell=0}(C^2S)_{\ell=0}(\theta^o_{\mathrm{p},\ell=0})^2 \\ &= 2(2.22\times10^6\,\mathrm{eV})(8.10\times10^{-3})(1.01)(0.45) = 16.3\,\mathrm{keV} \\ \Gamma^o_{\mathrm{p},\ell=2} &= 2\frac{\hbar^2}{mR^2}\,P_{\ell=2}(C^2S)_{\ell=2}(\theta^o_{\mathrm{p},\ell=2})^2 \\ &= 2(2.22\times10^6\,\mathrm{eV})(7.90\times10^{-5})(\approx 0)(0.45) \approx 0\end{aligned}$$

The values of $(\theta^o_{\mathrm{p},\ell=0})^2$ and $(\theta^o_{\mathrm{p},\ell=2})^2$ are obtained by interpolating the results for $^{12}\mathrm{C}+\mathrm{p}$ and $^{22}\mathrm{Na}+\mathrm{p}$ shown in Fig. 2.27. The estimated "observed" proton partial width is

$$\Gamma^o_{\mathrm{p}} = \Gamma^o_{\mathrm{p},\ell=0} + \Gamma^o_{\mathrm{p},\ell=2} = 16.3\,\mathrm{keV}$$

The calculated result is in excellent agreement with the experimental value of $\Gamma_{\mathrm{p}} = (18 \pm 2)$ keV that was directly measured in $^{17}\mathrm{F(p,p)}^{17}\mathrm{F}$ elastic scattering studies (Bardayan et al. 2000).

Example 2.3

The "observed" proton partial width for the s-wave ($\ell = 0$) resonance at a center-of-mass energy of $E_r = 214$ keV ($J^\pi = 1/2^+$) in $^{24}\mathrm{Mg(p,}\gamma)^{25}\mathrm{Al}$ was directly measured. The result is $\Gamma^o_{\mathrm{p},\ell=0} = (1.40 \pm 0.12)\times10^{-2}$ eV (Powell et al. 1999). Estimate the proton spectroscopic factor for the corresponding compound state.

First, we calculate the "observed" single-particle proton width from Eq. (2.200),

$$\begin{aligned}\Gamma^o_{\lambda pc} &= 2\frac{\hbar^2}{mR^2}\,P_c(\theta^o_{pc})^2 = 2(1.84\times10^6\,\mathrm{eV})(4.56\times10^{-8})(0.59) \\ &= 9.90\times10^{-2}\,\mathrm{eV}\end{aligned}$$

We obtain from Eq. (2.201)

$$(C^2S)_{\ell=0} = \frac{\Gamma^o_{\mathrm{p},\ell=0}}{\Gamma^o_{\lambda pc}} = \frac{(1.40\pm0.12)\times10^{-2}\,\mathrm{eV}}{9.90\times10^{-2}\,\mathrm{eV}} = 0.14\pm0.01$$

The result is in excellent agreement with the value of $(C^2S)_{\ell=0} = 0.14$ measured independently in the proton transfer reaction $^{24}\mathrm{Mg(}^3\mathrm{He,d)}^{25}\mathrm{Al}$ (Peterson and Ristinen 1975).

2.6 Continuum Theory

It is interesting to discuss the extreme case where a projectile approaching the target in a particular channel α is very unlikely to reappear in the entrance channel once it has penetrated into the nuclear interior. The condition is fulfilled, for example, if the number of open channels is very large. This is typically the case when the energy of the incident particle is much higher than the first few excitation energies of the target nucleus (say, $E > 3$ MeV for target masses of $A > 50$). The condition may also be fulfilled at low energies if the incident particle initiates a reaction with a large positive Q-value (say, $Q > 2$ MeV). In these cases we expect that, once the incident particle is inside the nucleus, it exchanges its energy rapidly with the other nucleons and the probability that it leaves by the same channel α is very small.

For simplicity, s-wave neutrons are considered again as incident particles. For the interior wave function we find from Eq. (2.142)

$$u_{\text{in}} \sim e^{-iKr} \tag{2.202}$$

It has the form of an ingoing wave only since it does not return. This is only a rough approximation since it is impossible to represent the motion of the incident particle inside the nucleus as a function of r only. However, it represents the main features of the dependence of the wave function on r. The logarithmic derivative of the radial wave function must be continuous at $r = R$. Hence (see Eq. (2.130))

$$f_0 = R\left(\frac{1}{u_{\text{in}}(r)}\frac{du_{\text{in}}(r)}{dr}\right)_{r=R} = R\frac{\left[\frac{d}{dr}(Be^{-iKr})\right]_{r=R}}{Be^{-iKr}} = -iKR \tag{2.203}$$

Substitution into Eq. (2.138) yields immediately for the reaction cross section (since $\text{Re}\, f_0 = 0$ and $\text{Im}\, f_0 = -KR$)

$$\sigma_{\text{re},0} = \frac{\pi}{k^2}\left(1 - \left|e^{2i\delta_0}\right|^2\right) = \frac{\pi}{k^2}\frac{4kK}{(K+k)^2} \tag{2.204}$$

The wave number inside the nucleus, K, is the only information regarding the interior which enters into this expression. Comparison to Eqs. (2.51) and (2.68) shows that the reaction cross section for s-wave neutrons can be interpreted as the product of the maximum cross section, π/k^2, and the s-wave transmission coefficient, $\hat{T}_0$,

$$\sigma_{\text{re},0} = \sigma_{\text{re},0}^{\max}\hat{T}_0 \tag{2.205}$$

where

$$\hat{T}_0 = 1 - \left|e^{2i\delta_0}\right|^2 \tag{2.206}$$

Since we assumed that the projectile is not re-emitted by the compound nucleus into the entrance channel α, the reaction cross section σ_{re} here is identical with the cross section $\sigma_{\alpha C}$ for the formation of the compound nucleus through channel α. Also, disregarding the possibility that the incident particle can return via the entrance channel means that Eq. (2.204) cannot give rise to resonances. For this reason, the above method for determining the cross section is referred to as *continuum theory*.

From Eq. (2.204) we can also estimate the s-wave reaction cross section for neutrons at low incident energies E. For $k \ll K$, the wave number K in the interior does not change much with variations in k (see Fig. 2.7) and one finds

$$\sigma_{\mathrm{re},0} = \frac{\pi}{k^2}\frac{4kK}{(K+k)^2} \approx \frac{4\pi}{Kk} \sim \frac{1}{k} \sim \frac{1}{v} \sim \frac{1}{\sqrt{E}} \tag{2.207}$$

where $p = \hbar k$ and v is the velocity of the incident neutron. The result is independent of the reaction mechanism and is referred to as $1/v$ *law* for reactions induced by s-wave neutrons. Reaction cross sections for ^{3}He(n,p)^{3}H, ^{6}Li(n,α)^{3}H and ^{10}B(n,α)^{7}Li are displayed in Fig. 4.15a. Below a neutron energy of ≈ 1 keV, the cross sections follow the $1/v$ law.

Equations (2.204)–(2.206) are obtained under the assumption of s-wave neutrons as incident particles. They can be easily generalized for any projectile and orbital angular momentum (Blatt and Weisskopf 1952). The cross section for the formation of the compound nucleus through channel α is then given by

$$\sigma_{\alpha C} = \frac{\pi}{k^2}\sum_{\ell}(2\ell+1)\hat{T}_\ell(\alpha) \tag{2.208}$$

where

$$\hat{T}_\ell(\alpha) = 1 - \left|e^{2i\delta_{\alpha\ell}}\right|^2 \tag{2.209}$$

is the transmission coefficient of channel α for orbital angular momentum ℓ and $\delta_{\alpha\ell}$ is the corresponding phase shift in channel α for elastic scattering by an appropriate potential. The potential must be complex for reactions to occur; otherwise the phase shift will be real and the transmission coefficient vanishes. This is consistent with our earlier discussion in Section 2.3.6. Transmission coefficients are usually calculated numerically from so-called *optical model potentials* which represent the average nuclear potential. For more information on optical model potentials, see Satchler (1990).

2.7 Hauser–Feshbach Theory

In Section 2.5 we considered the case where a reaction proceeds through an isolated narrow resonance. We will now discuss the other extreme situation. With increasing excitation energy in the compound nucleus, the resonances become broader and are located closer together. There is a continuous transition from sharp, isolated levels to the so-called continuum where levels overlap so much that little structure remains in the cross section. In other words, the cross section varies smoothly with energy. The reaction cross section, averaged over any resonance structure, is derived in the following.

The total angular momentum J and parity π of the compound nucleus will be conserved in a reaction (α,α'). The average cross section is then given by a sum of contributions from separate J and π,

$$\langle \sigma_{\mathrm{re}}(\alpha,\alpha') \rangle = \sum_{J\pi} \langle \sigma_{\mathrm{re}}(\alpha,\alpha') \rangle^{J\pi} \tag{2.210}$$

Recall that α denotes a pair of particles (including their state of excitation) in a particular channel (Section 2.5.5). Unprimed and primed quantities refer to the incoming and outgoing channel of the reaction, respectively. Next, we factor each term $\langle \sigma_{\mathrm{re}}(\alpha,\alpha') \rangle^{J\pi}$ into a cross section for compound nucleus formation through channel α and a branching ratio for decay into channel α',

$$\langle \sigma_{\mathrm{re}}(\alpha,\alpha') \rangle^{J\pi} = \sigma_{\alpha C}^{J\pi} \frac{G_{\alpha'}^{J\pi}}{\sum\limits_{\alpha''} G_{\alpha''}^{J\pi}} \tag{2.211}$$

The quantities $G_{\alpha}^{J\pi}$ represent probabilities for the decay into a specific outgoing channel, where the sum over α'' in the denominator is over all channels to which the compound nucleus can decay ($\sum_{\alpha''} G_{\alpha''}^{J\pi} = 1$). The factorization of the cross section in Eq. (2.211) reflects the independence of formation and decay of the compound nucleus while still fulfilling the requirement of total angular momentum and parity conservation. Substitution of the reciprocity theorem (see Eq. (2.14))

$$(2I_1+1)(2I_2+1)k_{\alpha}^2 \langle \sigma_{\mathrm{re}}(\alpha,\alpha') \rangle^{J\pi} = (2I_1'+1)(2I_2'+1)k_{\alpha'}^2 \langle \sigma_{\mathrm{re}}(\alpha',\alpha) \rangle^{J\pi} \tag{2.212}$$

into Eq. (2.211) gives

$$\frac{G_{\alpha'}^{J\pi}}{G_{\alpha}^{J\pi}} = \frac{(2I_1'+1)(2I_2'+1)k_{\alpha'}^2 \sigma_{\alpha' C}^{J\pi}}{(2I_1+1)(2I_2+1)k_{\alpha}^2 \sigma_{\alpha C}^{J\pi}} \tag{2.213}$$

where I_1 and I_2 are the spins of the particles in channel α. Summation over all channels α'' yields (since $\sum_{\alpha''} G^{J\pi}_{\alpha''} = 1$)

$$G^{J\pi}_{\alpha'} = \frac{(2I_1'+1)(2I_2'+1)k^2_{\alpha'}\sigma^{J\pi}_{\alpha'C}}{\sum\limits_{\alpha''}(2I_1''+1)(2I_2''+1)k^2_{\alpha''}\sigma^{J\pi}_{\alpha''C}} \tag{2.214}$$

For the formation of the compound nucleus one can use Eq. (2.208),

$$\sigma_{\alpha C} = \sum_{J\pi}\sigma^{J\pi}_{\alpha C} = \frac{\pi}{k^2_\alpha}\sum_\ell (2\ell+1)\hat{T}_\ell(\alpha) \tag{2.215}$$

Since the cross section is averaged over many overlapping resonances, we expect that the transmission coefficient does not depend on J. Therefore

$$\sigma_{\alpha C} = \frac{\pi}{k^2_\alpha}\sum_\ell (2\ell+1)\sum_{J=|\ell-s|}^{\ell+s}\sum_{s=|I_1-I_2|}^{I_1+I_2}\frac{2J+1}{(2I_1+1)(2I_2+1)(2\ell+1)}\hat{T}_\ell(\alpha) \tag{2.216}$$

The quantities I, s, and ℓ have the same meanings as in Section 2.5.5 and refer to a specific channel α. The factor in front of the transmission coefficient takes the number of different spin orientations into account (Section 2.5.5). Rearranging the order of summation yields

$$\sigma_{\alpha C} = \frac{\pi}{k^2_\alpha}\sum_{J\pi}\frac{2J+1}{(2I_1+1)(2I_2+1)}\sum_{s=|I_1-I_2|}^{I_1+I_2}\sum_{\ell=|J-s|}^{J+s}\hat{T}_\ell(\alpha) \tag{2.217}$$

Comparison of Eqs. (2.215) and (2.217) then gives

$$\sigma^{J\pi}_{\alpha C} = \frac{\pi}{k^2_\alpha}\frac{2J+1}{(2I_1+1)(2I_2+1)}\sum_{s\ell}\hat{T}_\ell(\alpha) \tag{2.218}$$

Combining Eqs. (2.210), (2.211), (2.214), and (2.218) results in

$$\begin{aligned}\langle\sigma_{\mathrm{re}}(\alpha,\alpha')\rangle &= \sum_{J\pi}(2I_1'+1)(2I_2'+1)k^2_{\alpha'}\frac{\sigma^{J\pi}_{\alpha C}\sigma^{J\pi}_{\alpha' C}}{\sum\limits_{\alpha''}(2I_1''+1)(2I_2''+1)k^2_{\alpha''}\sigma^{J\pi}_{\alpha''C}}\\ &= \frac{\pi}{k^2_\alpha}\sum_{J\pi}\frac{2J+1}{(2I_1+1)(2I_2+1)}\frac{\left[\sum\limits_{s\ell}\hat{T}_\ell(\alpha)\right]\left[\sum\limits_{s'\ell'}\hat{T}_{\ell'}(\alpha')\right]}{\sum\limits_{\alpha''}\sum\limits_{s''\ell''}\hat{T}_{\ell''}(\alpha'')}\end{aligned} \tag{2.219}$$

This is the *Hauser–Feshbach formula* for energy-averaged cross sections (Hauser and Feshbach 1952, Vogt 1968). The quantity α refers to the incoming channel of the reaction and thus I_1 and I_2 are the spins of the target and projectile, respectively. The sum over α'' is again over all channels that are energetically

accessible for the decay of the compound nucleus at the total energy in the entrance channel. The sums over J^π, ℓ, and s run over all values allowed by the selection rules for angular momentum coupling (Appendix B): π is positive or negative; $J = 0, 1, 2, \ldots$ for A even, or $J = \frac{1}{2}, \frac{3}{2}, \frac{5}{2}, \ldots$ for A odd; s takes on all integer values between $|I_1 - I_2|$ and $I_1 + I_2$; ℓ takes on all even values between $|J - s|$ and $J + s$ if the pair α has the same parity as π and all odd values otherwise. We assume here that the transmission coefficients are independent of the channel spin (that is, the potential has no spin–orbit term) and, therefore, the sum over s in Eq. (2.219) becomes a simple multiplicative factor. See Problem 2.6.

The transmission coefficients $\hat{T}_\ell(\alpha)$ are determined by complex phase shifts $\delta_{\alpha\ell}$ (see Eq. (2.209)) that are usually calculated numerically from optical model potentials (Section 2.6). Recall that these represent the average nuclear potential only. Consequently, the transmission coefficients describe the formation probability of single-particle levels. In other words, the reaction cross section calculated from Eq. (2.219) cannot account for the fine structure shown in Fig. 2.25, but corresponds to the average cross section shown as the thick solid line.

The Hauser–Feshbach theory is also applicable if a channel involves the emission or absorption of γ-rays (Cowan, Thielemann and Truran 1991). A correction must be applied to Eq. (2.219) because the processes of compound nucleus formation and decay are not completely independent of each other as can be shown by a more involved derivation of the Hauser–Feshbach formula using the resonance theory (Vogt 1968). This *width-fluctuation correction* enhances the cross section for weak reaction channels at the cost of stronger ones and is most important near thresholds, where additional channels become energetically accessible, and for reactions with few open channels.

Recall that α also specifies the state of excitation of a pair of particles in a particular channel. In practical applications one is mostly interested in cross sections obtained by summing or averaging over specific sets of excited states. For example, what is usually measured in the laboratory is the quantity $\langle \sigma_{\rm re}(\alpha, \alpha') \rangle$, with α representing the ground states of target and projectile, summed over excited states in the outgoing channel α'. Or, if the reaction takes place in a hot stellar plasma, $\langle \sigma_{\rm re}(\alpha, \alpha') \rangle$ must be averaged over excited states in the entrance channel α (Section 3.1.5). In such cases, Eq. (2.219) is still valid if each of the transmission coefficients in the numerator is replaced by sums of transmission coefficients over the excited states in question. In exceptional cases, all the final states for compound nucleus decay and their quantum numbers are experimentally known. The Hauser–Feshbach formula can then be applied with essentially no adjustable parameters. In most cases of practical interest, however, the compound nucleus may decay to levels beyond the highest excited state for which energy, spin, and parity are explicitly

known. The transmission coefficients in the numerator and denominator of Eq. (2.219) must then be modified to include terms that integrate a nuclear level density over the energy region beyond the known levels. This requires the development of expressions for the density of states as a function of excitation energy, spin, and parity. The evaluation of the overall cross section is then reduced to the problem of determining the required transmission coefficients and nuclear level densities. For a detailed discussion of these quantities in connection with the Hauser–Feshbach model see, for example, Rauscher et al. (1997) or Arnould and Goriely (2003).

Figure 2.29 shows as an example the cross section for the ^{64}Ni(p,γ)^{65}Cu reaction at bombarding energies between 1 and 4 MeV. The ^{64}Ni(p,n)^{64}Cu reaction has a Q-value of ≈ -2.5 MeV, which means that at a bombarding energy close to 2.5 MeV the neutron channel opens and the (p,n) reaction will start to compete with the (p,γ) reaction. Since the total incoming flux must be constant, the opening of a new reaction channel corresponds to a reduction of flux into all other reaction channels. As a result, the cross section of the (p,γ) reaction drops substantially at the neutron threshold, giving rise to a so-called *competition cusp*. The dashed curve in Fig. 2.29 was obtained by using Eq. (2.219) and is in qualitative agreement with the measurements. The theoretical description of the data is significantly improved if width fluctuation corrections are taken into account (solid line). A discussion of the Hauser–Feshbach model in the context of thermonuclear reaction rates is given in Section 3.2.7.

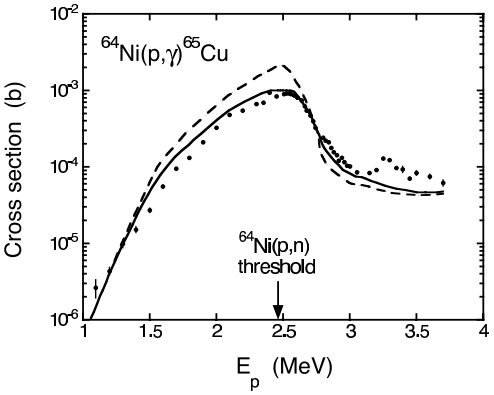

Fig. 2.29 Cross section versus bombarding energy for the ^{64}Ni(p,γ)^{65}Cu reaction. Beyond an energy of $\approx$ 2.5 MeV the endothermic ^{64}Ni(p,n)^{64}Cu reaction is energetically allowed. The sharp drop in the cross section at the neutron threshold reflects the decrease of the flux in all other decay channels of the compound nucleus ^{65}Cu. The curves show the results of Hauser–Feshbach statistical model calculations with (solid line) and without (dashed line) width fluctuation corrections. Reprinted from F. M. Mann et al., Phys. Lett. B, Vol. 58, p. 420 (1975). Copyright (1975), with permission from Elsevier.

Problems

2.1 Show by substituting Eq. (2.27) into Eq. (2.30) that the expansion coefficients are given by $b_\ell = (2\ell+1)i^\ell e^{i\delta_\ell}$. It is helpful for the derivation to write the sine functions as complex exponentials and to group separately the terms with e^{ikr} and e^{-ikr}.

2.2 The s-wave ($\ell = 0$) transmission coefficient at low energies compared to the Coulomb barrier height is given by Eq. (2.124). Derive the transmission coefficient at low energies for the Coulomb and centripetal potentials by substituting $V(r) = Z_0 Z_1 e^2/r + \ell(\ell+1)\hbar^2/(2mr^2)$ into Eq. (2.119). The simplest procedure is to expand the square root in the integrand before integration.

2.3 Suppose that a hypothetical resonance occurs in the A(p,γ)B reaction. The "observed" proton and γ-ray partial widths amount to Γ_p^o = 50 meV and Γ_γ^o = 50 meV, respectively. Assume that no other reaction channels are open. Use the one-level Breit–Wigner formula to calculate the ratio of reaction cross sections at E_r and $E_r + \Gamma^o$ (Γ^o denotes the total resonance width). Disregard the small energy dependence of the wave number k and of the partial widths.

2.4 Show explicitly that the general solution of Eq. (2.160) reduces for $\ell = 0$ neutrons to $u_0(r) = Ae^{ikr} + Be^{-ikr}$ (see Eq. (2.132)).

2.5 The E_r^{cm} = 518 keV ($J^\pi = 1^-$) s-wave resonance (Fig. 3.11) in the ^{13}C(p,γ)^{14}N reaction (Q = 7550 keV) has an "observed" proton and γ-ray partial width of Γ_p^o = 37 keV and Γ_γ^o = 9.4 eV, respectively, at the resonance energy. Both values are given here in the center-of-mass system. They are derived from the results reported in King et al. (1994). The latter value corresponds to the γ-ray partial width of the $E1$ transition to the ^{14}N ground state ($J^\pi = 1^+$). By using the energy dependences of the partial widths, find for this particular resonance the center-of-mass energy at which $\Gamma_p^o \approx \Gamma_\gamma^o$. Approximate the s-wave penetration factor by the Gamow factor and disregard the small energy dependence of the dimensionless single-particle reduced width.

2.6 Consider the ^{23}Na(p,α)^{20}Ne reaction, leading to the ^{20}Ne ground state ($J^\pi = 0^+$), at a center-of-mass proton energy of $E_\mathrm{p} \approx 0.4$ MeV [$J^\pi(^{23}\mathrm{Na}) = 3/2^+$, $J_\mathrm{p}^\pi = 1/2^+$]. The proton separation energy of ^{24}Mg (or the Q-value for the ^{23}Na(p,γ)^{24}Mg reaction) is S_p = 11.693 MeV (Audi, Wapstra and Thibault 2003). Hence, the compound nucleus ^{24}Mg has an excitation energy near 11.7 MeV + 0.4 MeV $\approx$ 12 MeV. At this energy, ^{24}Mg can decay by proton emission to the ^{23}Na ground state and by α-particle emission to the ^{20}Ne ground state or the ^{20}Ne first-excited state (E_x = 1.63 MeV, $J^\pi = 2^+$). Determine the energy-averaged cross section by writing down all terms of Eq. (2.219) up to and including $J = 2$.